Available online at www.sciencedirect.com
ScienceDirect
Deep-Sea Research I 55 (2008) 73–107
DEEP-SEA RESEARCH PART I
www.elsevier.com/locate/dsri

Influence of nutrient utilization and remineralization stoichiometry on phytoplankton species and carbon export: A modeling study at BATS

B. Salihoglu[a,b,*], V. Garçon[a], A. Oschlies[c], M.W. Lomas[d]

[a]*LEGOS/CNRS, Toulouse, France*
[b]*Institute of Marine Sciences, Middle East Technical University, Erdemli, Turkey*
[c]*IFM-GEOMAR, Kiel, Germany*
[d]*BIOS, Bermuda, USA*

Received 6 November 2006; received in revised form 13 September 2007; accepted 30 September 2007
Available online 22 October 2007

Abstract

The primary objective of this research is to understand the underlying mechanisms of the time-varying flux of carbon in the Sargasso Sea. To address this objective, a one-dimensional multi-component lower trophic level ecosystem model that includes detailed algal physiology as well as nutrient cycles is used at the Bermuda Atlantic Time-series Study (BATS, 31°40′N, 64°10′W) site. In this model autotrophic growth is represented by three algal groups and the cell quota approach is used to estimate algal growth and nutrient uptake. This model is tested and evaluated for year 1998 using the bimonthly BATS cruise data. Results show that phosphorus and dissolved organic matter (DOM) are necessary compartments to correctly simulate organic elemental cycles at the BATS site. Model results show that autotrophic eukaryotes and cyanobacteria (i.e. *Prochlorococcus* and *Synechococcus*) are the most abundant algal groups and are responsible for 63% and 33% of carbon production in the region, respectively. Sensitivity analyses show that the annual contribution of nitrogen fixation and atmospheric nitrogen deposition to new production is approximately 9% and 3%, respectively. However, the recycled nitrogen and phosphorus are important components of the ecosystem dynamics because sustained growth of algal groups depends on remineralized nutrients which accounts for 75% of the annual carbon production. Nutrient uptake and remineralization stoichiometry can play an important role in determining the surface ocean nutrient distribution. Model results suggest phosphate limitation even during the spring bloom. Phosphate may thus limit the growth of all algal groups throughout the year.

Keywords: Biogeochemical modeling; Nutrient cycle; Carbon cycle; Algal groups; BATS

1. Introduction

The Sargasso Sea denotes a region that is seasonally oligotrophic, exhibiting marked seasonal variability in biogeochemical processes (Michaels et al., 1994; Carlson and Ducklow, 1996). The

*Corresponding author. Present address: Institute of Marine Sciences, METU, P.O. Box 28, Erdemli 33731, Mersin, Turkey.
E-mail addresses: baris@ims.metu.edu.tr (B. Salihoglu), veronique.garcon@cnes.fr (V. Garçon), aoschlies@ifm-geomar.de (A. Oschlies), Michael.Lomas@bios.edu (M.W. Lomas).

0967-0637/$ - see front matter © 2007 Elsevier Ltd. All rights reserved.
doi:10.1016/j.dsr.2007.09.010

dominant feature is the spring bloom which is driven by inputs of new nutrients from winter mixing (Ryther and Menzel, 1960; Menzel and Ryther, 1961). New production during the spring bloom is believed to represent more than half of the total annual new production for this region (Michaels et al., 1994; Doney et al., 1996; Siegel et al., 1999). Eukaryotic pico- and nano-phytoplankton and *Synechococcus* dominate the phytoplankton community during this period (DuRand et al., 2001). Diatoms are typically a small component of the phytoplankton biomass in the Sargasso Sea (Nelson and Brzezinski, 1997; Lomas and Bates, 2004) and have rarely been found to bloom at Bermuda Atlantic Time-series Study (BATS, Steinberg et al., 2001), although elevated diatom populations have been observed to occur in summer-time cyclonic and mode-water eddies in this region (Sweeney et al., 2003; McGillicuddy et al., 2007). Knowledge of absolute and relative contributions of various components of microbial food web to total biomass can improve our understanding and modeling of the biogeochemical cycling of carbon and nutrients. In particular, food web structure and phytoplankton community distribution are important determinants of variability in carbon production and export from the euphotic zone. Thus, the first objective of this study is directed at understanding the influence of phytoplankton community on carbon production and export.

In the surface waters of the oligotrophic BATS station dissolved inorganic carbon (DIC) concentrations often decline through the summer despite the lack of nitrogen in the upper ocean, implying existence of nitrogen fixation, atmospheric inputs of nitrogen, significant deviations from the Redfield stoichiometry (Redfield et al., 1963), or some combination of these three mechanisms (Michaels et al., 1994; Capone et al., 2005). Nitrogen fixation has been recognized as a source of new nitrogen in the oligotrophic oceans for several decades. In the subtropical North Atlantic geochemical (indirect) estimates of annual rates of nitrogen fixation vary between 72 and 320 $\mathrm{mmol\,N\,m^{-2}\,yr^{-1}}$ (Michaels et al., 1996; Gruber and Sarmiento, 1997). However, these geochemical estimates are in contrast with the low rates ($0.25-34\,\mathrm{mmol\,N\,m^{-2}\,yr^{-1}}$) observed using biological (direct) estimates (Capone et al., 1997; Carpenter et al., 1999; Orcutt et al., 2001). A recent analysis where Hansell et al. (2004) combined the geochemical and direct biological estimates, suggested an intermediate value ($45\,\mathrm{mmol\,N\,m^{-2}\,yr^{-1}}$). The quantitative importance of this source of new nitrogen to the upper ocean remains uncertain (Gruber and Sarmiento, 2002; Lee et al., 2002; Hansell et al., 2004), especially given that the nitrogen fixing unicellular diazotrophic cyanobacteria and bacterioplankton can be important in some oligotrophic oceans (Zehr et al., 2001; Montoya et al., 2004). Recently, Spokes et al. (2000) argued that ~30% of new production can be supported by atmospheric inputs in the eastern Atlantic waters which, in geochemical estimates, leave the same trace as nitrogen fixation. Also Hastings et al. (2003) and Knapp et al. (2005) suggested that nitrogen fluxes other than nitrogen fixation and nitrate from below, such as precipitation, should be considered in the context of nitrogen mass balance. Although the average carbon:nitrogen:phosphorus (C:N:P) of organic particulate matter is close to the Redfield ratio, selected regions, depths, and seasons vary considerably in this regard (Hebel and Karl, 2001). This local and temporal variation in the elemental composition of particles could be linked to the composition and structure of the food webs (Geider and La Roche, 2002). The second objective of this study is to analyze the relative influence of these three mechanisms (nitrogen fixation, atmospheric inputs of nitrogen, deviations from the Redfield stoichiometry) on organic carbon production and export.

Although recent studies point toward phosphorus deficiency relative to nitrogen (Tyrell, 1999; Wu et al., 2000; Lipschultz et al., 2002; Ammerman et al., 2003; Lomas et al., 2004), the role of phosphorus has, so far, been largely ignored in subtropical Atlantic waters. We speculate that this could even lead to a re-evaluation of the traditional picture of the Atlantic Ocean as a region in which phytoplankton growth is predominantly controlled by the availability of nitrogen and sometimes silicate. The third objective of this paper focuses on investigating the influence of phosphorus on the Sargasso Sea ecosystem by incorporating both nitrogen and phosphorus cycles in a relatively complex model that includes detailed algal physiology.

2. Model structure

In this study a one-dimensional, algal group (AG)-based phytoplankton model (e.g. Salihoglu and Hofmann, 2007) is used to simulate phytoplankton dynamics in the upper 200 m of the Sargasso Sea at

the BATS site. The phytoplankton model is coupled to a larger model structure that provides a simulated underwater light field which drives phytoplankton primary production via a bio-optical model. Details of the algal group model and the irradiance model are given in Salihoglu (2005) and only the modifications on this model which include changes on algal group, nutrient, zooplankton, and detritus compartments will be described here.

The phytoplankton algal groups (AG) included as state variables in the ecosystem model (Fig. 1) represent the dominant autotrophic biomass in the Sargasso Sea as determined from pigment and size fractional studies (Gin et al., 1999; DuRand et al., 2001). The first cyanobacteria group corresponds to *Prochlorococcus* and *Synechococcus* species given in Salihoglu and Hofmann (2007). This is the smallest size group, ~0.9 μm, which accounts for a significant fraction of carbon biomass (i.e. ~37% of photosynthetic carbon standing stock) in the Sargasso Sea waters (DuRand et al., 2001). Autotrophic eukaryotes which are larger than the first group have been referred to as picoeukaryotes (Campbell and Vaulot, 1993), nanoeukaryotes (Landry et al., 1995), and eukaryotic ultraplankton (Li et al., 1993). This group, ~2.5 μm, accounts for the largest fraction of the carbon biomass (52–65%) in the region (DuRand et al., 2001). The third algal group includes (~15 μm cell size) diatoms. *Trichodesmium* species is not explicitly included in this model structure, given the limited carbon production by this species at BATS (Orcutt et al., 2001), but nitrogen fixation by this species is implicitly included as described in Section 2.3.

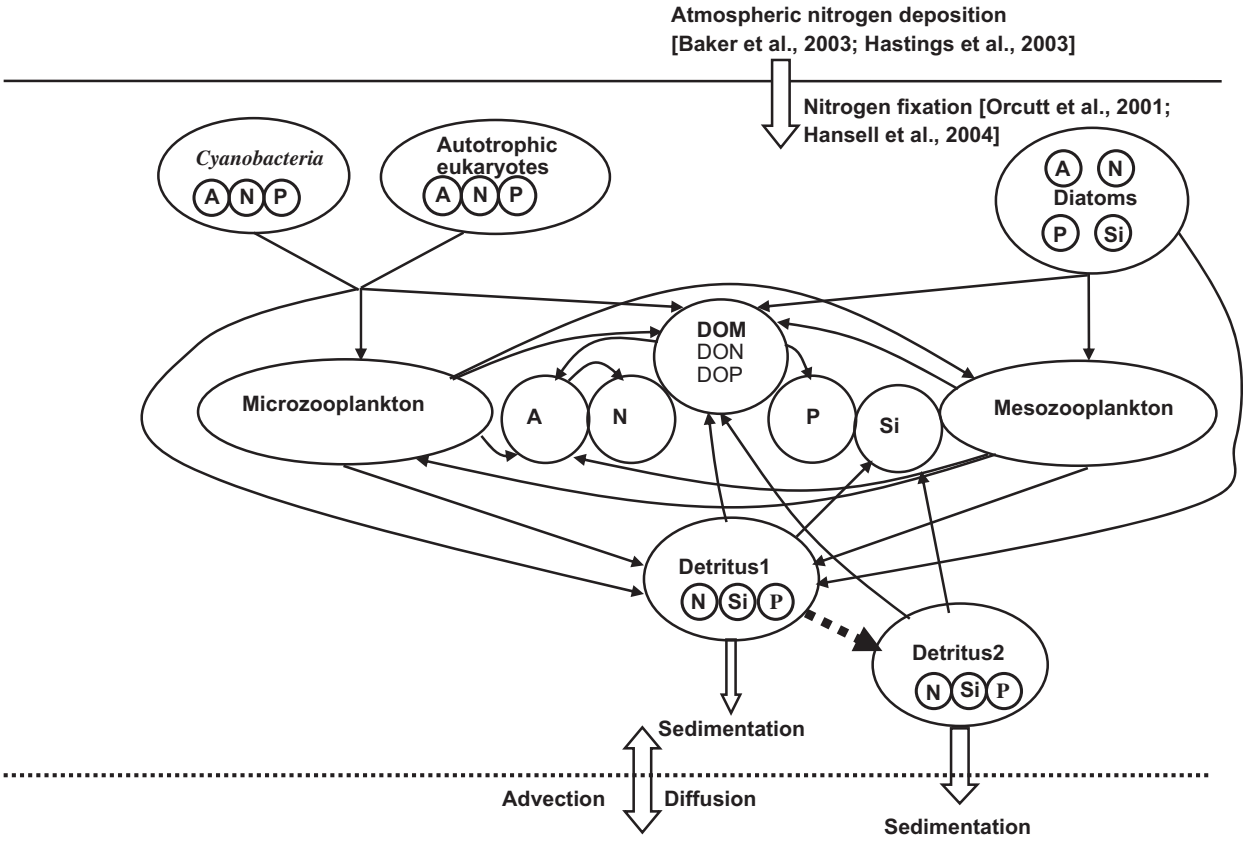

Fig. 1. Schematic of the lower trophic level ecosystem model components. Small circles inside the big circles indicate the internal nutrient compartments of each algal and detrital group. Interactions between nutrient, phytoplankton, zooplankton, and detritus compartments are shown by solid lines and arrows. Small arrows indicate the direction of transfer between model compartments, open arrows indicate the direction of transfer at the model boundaries. The dashed arrow indicates aggregation of small detritus to large detritus. The upper model boundary is indicated by a solid line, and it is only open to aeolian nitrogen deposition. The bottom boundary is an open boundary which is indicated by a dotted line. Abbreviations used are: A—ammonium; N—nitrate; P—phosphate; Si—silicate; DOM—dissolved organic matter; DON—dissolved organic nitrogen; DOP—dissolved organic phosphorus.

Currently it is being discussed that nitrogen and phosphorus may limit primary production in the Sargasso Sea (Fanning, 1992; Wu et al., 2000; Lipschultz et al., 2002; Lomas et al., 2004) and that silicate may limit diatom growth (Brzezinski and Nelson, 1996; Lima and Doney, 2004). This understanding is included in the formulations used for growth of the three algal groups, which incorporates uptake of ammonium, nitrate, phosphate, and silicate. Another debate is on nitrate utilization by *Prochlorococcus*. Previous culture studies showed that *Prochlorococcus* is not able to use nitrate but grows well on ammonium (Moore et al., 2002). However, a recent study by Casey et al. (2007) has shown that this understanding may need to be re-evaluated because some ecotypes of *Prochlorococcus* present in the ocean but not represented by cultured isolates can assimilate nitrate. Based on these studies, in the model, all of the algal groups use ammonium and phosphate (Fig. 1), whereas nitrate uptake by the first algal group is assumed to be highly limited. Silicate is used only by algal group 3.

Each algal group has cellular carbon, nitrogen, and phosphorus compartments and algal group 3 has a cellular silicon compartment. The phytoplankton cellular nitrogen, phosphorus, and silicon are needed to calculate uptake of nitrogen, phosphorus, and silicon by phytoplankton and to estimate nitrogen-, phosphorus-, and silicon-limited growth rates. Recent studies show maximum cellular cyanobacteria C:N ratios are lower (7.4) (Bertilsson et al., 2003) compared to autotrophic eukaryotes (11) and microphytoplankton (13) (Geider et al., 1998; Leonardos and Geider, 2004). Maximum cellular cyanobacteria C:P ratio is much higher (464) (Bertilsson et al., 2003) compared to autotrophic eukaryotes (128) and diatoms (110) (Ho et al., 2003; Leonardos and Geider, 2004). This structure is included in the model formulations.

The chlorophyll *a* equations are linked to cellular carbon, nitrogen, and phosphorus state equations by variable cellular carbon to chlorophyll *a*, nitrogen to chlorophyll *a*, and phosphorus to chlorophyll *a* ratios. Carbon to chlorophyll *a* ratios of each algal group are estimated using the procedure given in Bissett et al. (1999b) and explained in detail in Salihoglu (2005).

Over the past three decades it has been recognized that dissolved organic substrates are important intermediates in cycling of bioactive elements within the ocean (Hedges, 2002). Large amounts of nutrients can be made available in the upper ocean by rapid cycling of dissolved organic matter (DOM, Pomeroy, 1974; Azam and Hodson, 1977) released by a variety of processes including phytoplankton exudation, bacterial release, viral lysis, zooplankton excretion and grazing (Jumars et al., 1989; Nagata, 2000; Carlson, 2002), and mechanical breakdown and subsequent dissolution of detritus and fecal pellets (Jumars et al., 1989; Lampitt, 1990; Strom et al., 1997). Several modeling studies (Fasham et al., 1990; Spitz et al., 2001; Anderson and Pondaven, 2003) also showed that including dissolved organic nitrogen (DON) dynamics can improve model performance in the Sargossa Sea. The cycling of DOM (i.e. DON and DOP) is included in the model and the breakdown of DOM by bacteria is parameterized as a function of temperature (cf. Sections 2.3 and 2.4).

Two groups of zooplankton are included in the ecosystem model. The first group represents microzooplankton, which includes phagotrophic protists, and small animals that pass through a 200 μm mesh net (Landry et al., 1995). The second group, the mesozooplankton, includes 200 to 2000 μm size animals (mostly copepods) (Dam et al., 1995; Madin et al., 2001). In this model, microzooplankton graze on cyanobacteria and autotrophic eukaryotes (Fig. 1). The mesozooplankton graze on large phytoplankton and microzooplankton (Dam et al., 1995; Landry et al., 1995; Zhang et al., 1995; Verity et al., 1996).

The detrital component of the ecosystem model is divided into small (Detritus1, Fig. 1) and large (Detritus2, Fig. 1) detritus groups. Detrital components are split into two groups because each group has unique sinking and remineralization rates (Nelson et al., 1995; Laws et al., 2000). The small detrital pool receives inputs from algal groups 1–3 that results from losses due to non-grazing mortality and unassimilated grazed fraction. Additional inputs to this detrital pool are from zooplankton mortality. Remineralization of small and large detritus provides sources for DON and DOP (Jumars et al., 1989). Dissolution of silicate in the detritus compartment provides a source for this nutrient (Nelson et al., 1995). In this model small detritus aggregates into large detritus and the aggregation rate increases as a function of small detritus concentration (Jackson and Burd, 1998). Large detritus is assumed to sink faster than small detritus.

Forcing by the physical environment is provided by vertical advection, diffusion, and mixing. This

forcing acts on all model state variables. The detritus compartments are also allowed to sink at a fixed rate.

2.1. Phytoplankton state equations

The basic state equation governing phytoplankton dynamics for each algal group (AG_i) is of the form

$$\frac{\partial AG_i}{\partial t} + w\frac{\partial AG_i}{\partial z} - \frac{\partial}{\partial z}K_z\frac{\partial AG_i}{\partial z} = [\min(\mu_{ll_i}, \mu_{nul_i})]AG_i - m_i AG_i - I_{AG_i}Z_{s+l} \quad \text{for } i = 1, 3, \tag{1}$$

where the three terms on the left side represent changes in each algal group that are produced by local time (t) variations, vertical (z), advection (w), and vertical diffusive flux (K_z), respectively. The right side of Eq. (1) represents the biological processes that provide sources and sinks of each algal group, which includes light- (μ_{ll_i}) and nutrient-limited (μ_{nul_i}) growth, natural mortality (m_i), and losses due to microzooplankton and mesozooplankton (Z_{s+l}) grazing, respectively. All of the phytoplankton growth and loss processes are expressed in terms of carbon. The definitions and units of the parameters used in the algal group equations are given in Table 1.

The realized net growth rate for each algal group, $\mu_i = [\min(\mu_{ll_i}, \mu_{nul_i})]$, is the minimum of the light- and nutrient-limited growth rates, which limits growth by the least available resource (e.g. Walsh, 1975). The basal growth rate, on which μ_{ll_i} and μ_{nul_i} are based, is determined from temperature (T) using the specific growth relationship given by Eppley (1972), which is of the form

$$\mu_{mt_i}(z, t) = \mu_{m_i}\exp^{0.0633(T(z)-27)}, \tag{2}$$

Table 1
Definitions and units of variables or parameters used in the equations that describe the dynamics of phytoplankton particulate carbon, nitrogen, phosphorus, and silicon for each algal group

Symbol	Definition	Units
μ_{ll}	Light-limited carbon-specific growth rate	h^{-1}
μ_{nul}	Nutrient-limited carbon-specific growth rate	h^{-1}
m	Phytoplankton-specific death rate	h^{-1}
μ_{mt}	Maximum, temperature-dependent carbon-specific growth rate	h^{-1}
μ_m	Maximum, 24 h, carbon-specific growth rate at 27 °C	d^{-1}
g_{AG}	Phytoplankton-specific grazing coefficient	d^{-1}
Λ	Ivlev coefficient of grazing	$(mmol\,C\,m^{-3})^{-1}$
$\rho_{NO_3^-}$	Absolute nitrate transport flux	$\mu mol\,N\,l^{-1}\,d^{-1}$
$\rho_{NH_4^+}$	Absolute ammonium transport flux	$\mu mol\,N\,l^{-1}\,d^{-1}$
$\rho_{PO_4^{3-}}$	Absolute phosphate transport flux	$\mu mol\,P\,l^{-1}\,d^{-1}$
ρ_{Si}	Absolute silicate transport flux	$\mu mol\,Si\,l^{-1}\,d^{-1}$
$K_{sNO_3^-}$	Half saturation constant for nitrate uptake	$\mu mol\,NO_3^-\,l^{-1}$
ψ	Nitrate uptake repression exponent	$(\mu mol\,NH_4^+\,l^{-1})^{-1}$
$K_{sNH_4^+}$	Half saturation constant for ammonium uptake	$\mu mol\,NO_3^-\,l^{-1}$
$K_{sPO_4^{3-}}$	Half saturation constant for phosphate uptake	$\mu mol\,PO_4^{3-}\,l^{-1}$
K_{sSi}	Half saturation constant for silicate uptake	$\mu mol\,Si\,l^{-1}$
$\overline{\mu}$	Growth rate at maximum cellular nutrient concentrations	d^{-1}
K_{QN}	Subsistence quota for nitrogen-limited growth	$\mu mol\,N\,(\mu mol\,C)^{-1}$
Q_N	Cellular nitrogen status of the algal group	$\mu mol\,N\,(\mu mol\,C)^{-1}$
K_{QP}	Subsistence quota for phosphorus-limited growth	$\mu mol\,P\,(\mu mol\,C)^{-1}$
Q_P	Cellular phosphorus status of the algal group	$\mu mol\,P\,(\mu mol\,C)^{-1}$
K_{QSi}	Subsistence quota for silicate-limited growth	$\mu mol\,Si\,(\mu mol\,C)^{-1}$
Q_{Si}	Cellular silicate status of the algal group	$\mu mol\,Si\,(\mu mol\,C)^{-1}$
QN_{max}	Maximum allowed nitrogen to carbon ratio in each algal group	$\mu mol\,N\,(\mu mol\,C)^{-1}$
QP_{max}	Maximum allowed phosphorus to carbon ratio in each algal group	$\mu mol\,P\,(\mu mol\,C)^{-1}$
QSi_{max}	Maximum allowed silicate to carbon ratio in each algal group	$\mu mol\,Si\,(\mu mol\,C)^{-1}$

Table 2
Values of parameters, defined in Table 1, used in the equations describing the dynamics of each algal group (AG)

Parameter	AG1	AG2	AG3
m	0.1^{1}	0.1^{1}	0.1^{1}
μ_m	$0.68^{2,3,4,5}$	1.2^{6}	1.66^{6}
g_{AG}	$4^{7,8}$	$4^{7,8}$	$5^{9,10}$
$K_{s\mathrm{NO_3}}$	$0.13^{11,12}$	0.417^{12}	2.29^{13}
$K_{s\mathrm{NH_4}}$	$0.065^{11,12}$	0.208^{12}	2.18^{13}
$K_{s\mathrm{P}}$	0.008^{14}	0.026^{15}	0.143^{12}
$K_{s\mathrm{Si}}$	–	–	1.2^{16}
$K_{Q\mathrm{N}}$	$7.4^{-1^{5}}$	$11.00^{-1^{11,17,18,19}}$	$13^{-1^{20}}$
$K_{Q\mathrm{P}}$	$464^{-1^{21}}$	$128^{-1^{22}}$	$110^{-1^{23,24}}$
$K_{Q\mathrm{Si}}$	–	–	0.18^{25}
$Q\mathrm{N}_{\max}$	$5.2^{-1^{5}}$	$5.5^{-1^{11,17,18,19}}$	$5.25^{-1^{20}}$
$Q\mathrm{P}_{\max}$	$143^{-1^{21}}$	$27^{-1^{22}}$	$50^{-1^{23,24}}$
$Q\mathrm{Si}_{\max}$	–	–	0.315^{25}

Superscripts refer to the references that provide the source for the parameter value and the citations are as follows: [1]Leonard et al. (1999); [2]Moore et al. (1995); [3]Partensky et al. (1993); [4]Cuhel and Waterbury (1984); [5]Kana and Glibert (1987); [6]Sunda and Huntsman (1995); [7]Landry et al. (1995); [8]Verity et al. (1996); [9]Dam et al. (1995); [10]Roman and Gauzens (1997); [11]Harrison et al. (1996); [12]see text for calculations; [13]Zhang and Zou (1997); [14]Timmermans and et al. (2005); [15]Parpais et al. (1996); [16]Nelson and Treguer (1992); [17]Laws and Bannister (1980); [18]Sakshaug et al. (1989); [19]Flynn et al. (1994); [20]Geider et al. (1998); [21]Bertilsson et al. (2003); [22]Geider and La Roche (2002); [23]Ho et al. (2003); [24]Leonardos and Geider (2004); [25]Takeda (1998). The parameters that are not required by a particular algal group are indicated by—.

where $T(z)$ is temperature in °C, μ_{mt_i} is the temperature-dependent maximum growth rate for each algal group, and μ_{m_i} is the maximum growth rate at 27 °C for each algal group (Table 2). Details of the formulations used to obtain the light-limited growth rate μ_{ll_i} are given in Salihoglu and Hofmann (2007) and the nutrient-limited growth μ_{nul_i} is explained below.

Losses due to grazing by zooplankton are obtained using the formulation given by Franks et al. (1986) which is of the form

$$I_{\mathrm{AG}_i} = g_{\mathrm{AG}_i} \Lambda \mathrm{AG}_i (1 - \mathrm{e}^{-\Lambda \mathrm{AG}_i}), \tag{3}$$

where g_{AG_i} is the maximum grazing rate of zooplankton on each algal group (Table 2) and Λ is the Ivlev (1955) coefficient for zooplankton grazing (Table 3).

Phytoplankton particulate nitrogen, phosphorus, and silicon are integral components of the dynamics governing each algal group because they affect both nutrient uptake and nutrient-limited growth rates of each algal group. The equation for phytoplankton particulate phosphorus (AGP_i) is given here as example:

$$\frac{\partial \mathrm{AGP}_i}{\partial t} = \rho_{\mathrm{PO_4}i} - m_i \mathrm{AGP}_i - I_{\mathrm{AGP}_i} \left[Z_s \left(\frac{\mathrm{P}}{\mathrm{C}} \right)_{Z_s} + Z_l \left(\frac{\mathrm{P}}{\mathrm{C}} \right)_{Z_l} \right]. \tag{4}$$

The physical processes (i.e. vertical advection and diffusion) are the same as given in Eq. (1) and from now on, for all state variables, they will not be repeated. The first term on the right side of Eq. (4) represents increases in algal group particulate phosphorus resulting from phosphorus uptake. The second and third terms represent losses from the particulate phosphorus pool by natural mortality of each algal group and grazing by microzooplankton and mesozooplankton, represented by Z_s and Z_l, respectively. The particulate carbon pools of each zooplankton group are converted to a phosphorus equivalent using a phosphorus to carbon ratio (P/C), for the respective group. This ratio is estimated by tracking the phosphorus to carbon ratio in the phytoplankton grazed by each zooplankton group, and it is calculated at each time step and at each depth.

The nutrient-limited growth rate (μ_{nul_i} in Eq. (1)) was formulated using separate parameterizations for nutrient uptake and growth rates. For example, the rate at which the different algal groups take up phosphate (first term, right side of Eq. (4)) is related via a Monod function to the ambient phosphate concentration as

$$\rho_{\mathrm{PO_4^{3-}}i}(z,t) = \mu_{mt_i}(z,t) \mathrm{AGP}_i \left[\frac{\mathrm{PO_4^{3-}}}{K_{s\mathrm{PO_4^{3-}}i} + \mathrm{PO_4^{3-}}} \right], \tag{5}$$

where the maximum rate of uptake is determined by the temperature-dependent-specific growth rate ($\mu_{mt_i}(z,t)$), and the phosphate concentration at which one-half the maximum rate is obtained as given by $K_{s\mathrm{PO_4^{3-}}i}$ (Table 2). The rate of phosphate uptake is also modified by the particulate phosphorus concentration of each algal group (AGP_i).

The effect of cellular nutrient concentrations on the nutrient-limited growth rate ($\mu_{\mathrm{nul}_i}(z,t)$) of the carbon-based biomass was included using a Droop (1973) equation which provides a realistic mathematical representation of growth under nutrient limiting conditions (Marra et al., 1990; Haney and

Table 3
Definitions, values, and units of the parameters used in the zooplankton, nutrient, and detritus governing equations

Symbol	Definition	Value	Units
Λ	Ivlev coefficient of grazing	1[1]	$(\text{mmol C m}^{-3})^{-1}$
e_s	Mesozooplankton excretion rate	0.1[2,3,4]	d^{-1}
m_{Z_s}	Mesozooplankton death rate	0.6	d^{-1}
e_l	Microzooplankton excretion rate	0.1[2,3,4]	d^{-1}
m_{Z_l}	Microzooplankton death rate	0.5	d^{-1}
λ^*	Zooplankton assimilation efficiency	0.75[1]	Unitless
g_{Z_s}	Mesozooplankton-specific grazing coefficient	15[5,6]	d^{-1}
nitr	Nitrification rate of ammonium to nitrate	0.05[7]	d^{-1}
FN	Aeolian nitrogen deposition at the surface	Estimated	$\mu\text{mol N m}^{-2}\,\text{d}^{-1}$
Nfix	Nitrogen fixation	Estimated	$\mu\text{mol N m}^{-2}\,\text{d}^{-1}$
c_{a}^*	Remineralization rate of DON to ammonium	0.018[8]	d^{-1}
c_{P}^*	Remineralization rate of DOP to phosphate	0.018[8,9,10]	d^{-1}
c_{Si}^*	Dissolution rate of detritus to silicate	0.1[11]	d^{-1}
c_{DON}^*	Remineralization rate of detritus to DON	0.16[8,12]	d^{-1}
c_{DOP}^*	Remineralization rate of detritus to DOP	0.16[8,9,10]	d^{-1}
sc_{des}	Small detritus sinking rate	2[8]	m d^{-1}
sc_{del}	Large detritus sinking rate	30[8]	m d^{-1}
agg	Aggregation rate of small detritus to large detritus	0.01[13]	d^{-1}
c_{c}^*	Remineralization rate of detritus to carbon	0.1[8]	d^{-1}

Superscripts refer to the references that provide the source for the parameter value and the citations are as follows: [1]Leonard et al. (1999); [2]Landry et al. (1996); [3]Hutchins and Bruland (1995); [4]Steinberg et al. (2000); [5]Dam et al. (1995); [6]Roman et al. (2002); [7]see text for calculations; [8]Laws et al. (2000); [9]Karl and Bjorkman (2002); [10]Benitez-Nelson (2000); [11]Nelson et al. (1995); [12]Bronk (2002); [13]Jackson and Burd (1998).

Jackson, 1996) and is of the form

$$\mu_{\text{nul}_i}(z,t) = \overline{\mu_i}(z,t)\left[1 - \frac{K_{Q\text{N}_i}}{Q_{\text{N}_i}(z,t)}\right] \times \left[1 - \frac{K_{Q\text{P}_i}}{Q_{\text{P}_i}(z,t)}\right]\left[1 - \frac{K_{Q\text{Si}_3}}{Q_{\text{Si}_3}(z,t)}\right], \quad (6)$$

where $\overline{\mu_i}(z,t)$ is the algal group growth rate that occurs at maximum ratios of algal group particulate nitrogen to carbon ($\text{AGN}_i : \text{AG}_i$), particulate phosphorus to carbon ($\text{AGP}_i : \text{AG}_i$), and particulate silicon to carbon ($\text{AGS}i_3 : \text{AG}_3$) ratios. The actual algal group particulate nitrogen to carbon, particulate phosphorus to carbon, and particulate silicon to carbon ratios are represented by $Q_{\text{N}_i}(z,t)$, $Q_{\text{P}_i}(z,t)$, and $Q_{\text{Si}_3}(z,t)$ (note that silicate is only limiting for AG3), respectively. The subsistence algal nitrogen, phosphorus, and silicon to carbon ratios are given by $K_{Q\text{N}_i}$, $K_{Q\text{P}_i}$, and $K_{Q\text{Si}_3}$, respectively. These subsistence quotas define the algal particulate nitrogen, phosphorus, and silicon to carbon ratios ($Q_{\text{N}_i}(z,t)$, $Q_{\text{P}_i}(z,t)$, and $Q_{\text{Si}_3}(z,t)$), where zero growth rate for each algal group occurs (Droop, 1973), and values for these are given in Table 2.

Here the actual cellular phosphorus to carbon ratio that controls the phosphorus-based algal growth rate is given as an example and is of the form

$$Q_{\text{P}_i}(z,t) = \frac{\text{AGP}_i}{\text{AG}_i}. \quad (7)$$

The actual growth rate (μ_{mt}) uses a true maximum growth rate ($\overline{\mu_i}$) which is reached when the algal group particulate nitrogen to carbon, particulate phosphorus to carbon, and particulate silicon to carbon ratios are maximized. Because μ_{mt} changes with time and depth, $\overline{\mu_i}$ is calculated for each time and depth from

$$\overline{\mu_i}(z,t) = \mu_{mt_i}(z,t)\left[1 - \frac{K_{Q\text{N}_i}}{Q\text{N}_{\max_i}}\right]^{-1} \times \left[1 - \frac{K_{Q\text{P}_i}}{Q\text{P}_{\max_i}}\right]^{-1}\left[1 - \frac{K_{Q\text{Si}_3}}{Q\text{Si}_{\max_3}}\right]^{-1}, \quad (8)$$

which is a modified form of Eq. (6) in which the maximum particulate nitrogen to carbon, phosphorus

to carbon, and silicon to carbon ratios for each algal group are used, which are given by $Q\mathrm{N}_{\max_i}$, $Q\mathrm{P}_{\max_i}$, $Q\mathrm{Si}_{\max_3}$, respectively (Table 2). Whenever these maximum ratios are exceeded during the simulations the excess cellular nitrogen and phosphorus are assumed to be exudated as DON and DOP, whereas uptake of silicate stops when silicate to carbon ratios reach their maximum.

2.2. Zooplankton state equations

The governing equation for microzooplankton (Z_s) is assumed to be of the form

$$\frac{\partial Z_s}{\partial t} = \sum_{i=1}^{2} \lambda^* I_{\mathrm{AG}_i} Z_s - I_{Z_s} Z_l - e_s Z_s - m_{z_s} Z_s. \qquad (9)$$

The terms on the right side of Eq. (9) are assimilated ingestion of grazed phytoplankton biomass, grazing on microzooplankton by mesozooplankton, excretion, and mortality, respectively.

The grazed biomass is assimilated with an efficiency given by λ^* (Table 3). Removal of microzooplankton by mesozooplankton grazing (I_{Z_s}) is parameterized in a manner similar to that used for grazing on phytoplankton (Eq. (3)) with microzooplankton-specific grazing rate (g_{Z_s}) and Ivlev constant (Λ).

The microzooplankton excretion loss rate is given by e_s. The microzooplankton mortality rate (m_{z_s}, Table 3) is such that 50% of the microzooplankton biomass is removed each day.

The equation governing the mesozooplankton (Z_l) dynamics is similar to Eq. (9) and is of the form

$$\frac{\partial Z_l}{\partial t} = \lambda^* I_{\mathrm{AG}_3} Z_l + \lambda^* I_{Z_s} Z_l - e_l Z_l - m_{z_l} Z_l. \qquad (10)$$

Increases in mesozooplankton biomass are supported by grazing on diatoms (AG3) and microzooplankton. Losses to the mesozooplankton biomass occur via excretion and mortality. Microzooplankton and mesozooplankton excretion of nitrogen is equally distributed among ammonium and DON pools and phosphorus excretion enters the DOP pool (cf. Sections 2.3 and 2.4). The mesozooplankton mortality m_{z_l} (Table 3) includes natural as well as predation mortality.

2.3. Nutrient state equations

Inorganic nitrogen is partitioned into two components, recycled nitrogen, ammonium, and new nitrogen, nitrate. The state equation governing the nitrate dynamics is of the form

$$\frac{\partial \mathrm{NO}_3^-}{\partial t} = -\sum_{i=1}^{3} \rho_{\mathrm{NO}_3^- i} + \mathrm{nitr} + \delta(z)(\mathrm{FN} + \mathrm{Nfix}). \qquad (11)$$

The first term on the right is nitrate uptake by each phytoplankton algal group, and the first gain term is the nitrification (nitr) which transfers ammonium to nitrate at a constant rate (Table 3). Recent evidence suggests that a major fraction of nitrate could arise from euphotic zone nitrification (Dore and Karl, 1996; Lipschultz, 2001; Lipschultz et al., 2002). Therefore, in this study it is assumed that ammonium is converted to nitrate at a rate of $0.05\,\mathrm{d}^{-1}$, and the influence of light inhibition is not included. This value is also used in a recent modeling study by Mongin et al. (2003). The last term is the atmospheric (aeolian) deposition of nitrate (FN) and nitrogen fixation (Nfix) which provide another input for the lower trophic level ecosystem model (Fig. 1). Atmospheric nitrate deposition is based on observations and both wet (Hastings et al., 2003) and dry (Baker et al., 2003) depositions are considered. Because no major seasonal variation in nitrogen deposition is observed (Baker et al., 2003; Hastings et al., 2003) a constant daily wet ($19\,\mu\mathrm{mol\,N\,m^{-2}\,d^{-1}}$) and dry ($20\,\mu\mathrm{mol\,N\,m^{-2}\,d^{-1}}$) deposition is assumed. Nitrogen fixation is also based on the observed values which are obtained from Orcutt et al. (2001) and Hansell et al. (2004). The strong annual variability observed in nitrogen fixation is included in the model following the observations by Orcutt et al. (2001); however, the mean nitrogen fixation value is taken from Hansell et al. (2004) which is three times ($0.045\,\mathrm{mol\,N\,m^{-2}\,y^{-1}}$) the mean rate measured by Orcutt et al. (2001). The estimates by Orcutt et al. (2001) were during a predominantly negative North Atlantic Oscillation (NAO) period (1995–1997), therefore were biased toward lower values (Bates and Hansell, 2004). This yearly mean value is distributed over 1 year using the trichome abundance distribution (colony-equivalents m^{-2}) which is fitted as a third degree polynomial function of year days (x); trichome abundance $= -1.7 + 0.7x + 0.1x^2 - 0.0003x^3$ (following Orcutt et al., 2001). The aeolian nitrogen deposition and nitrogen fixation are applied only at the surface ($\delta[z=0] = 1$; $\delta[z>0] = 0$) and are subsequently mixed vertically (cf. Section 3.1). This assumption is based on

the observations by Orcutt et al. (2001), which showed that most of the nitrogen fixation occurs in surface colonies. Recently, Davis and McGillicudy (2006) showed that nitrogen fixation below surface can be higher than that reported by Orcutt et al. (2001) but it can also be expected to be a function of light level which decreases exponentially with depth.

The state equation of ammonium is of the form

$$\frac{\partial \mathrm{NH}_4^+}{\partial t} = \sum_{i=1}^{3}(-\rho_{\mathrm{NH}_{4_i}^+}) - \mathrm{nitr} + 0.5e_s Z_s \left(\frac{\mathrm{N}}{\mathrm{C}}\right)_{Z_s} + 0.5e_l Z_l \left(\frac{\mathrm{N}}{\mathrm{C}}\right)_{Z_l} + c_{\mathrm{a}}\mathrm{DON}. \quad (12)$$

The biological processes represented by the terms on the right side of Eq. (12) are uptake by each algal group, nitrification, excretion by microzooplankton, excretion by mesozooplankton, and remineralization of DON. The particulate carbon pools of each zooplankton group are converted to a nitrogen equivalent using a nitrogen to carbon ratio (N/C) for each group to estimate the amount of nitrogen in the excretion. This ratio is estimated by tracking the nitrogen to carbon ratio in the phytoplankton grazed by each zooplankton group, and it is calculated at each time and depth. In this study it is assumed that 50% of the excreted nitrogen joins the ammonium pool (Bidigare, 1983). The remineralization rate of DON to ammonium, $c_{\mathrm{a}}(z)$, is assumed to be modified by temperature as

$$c_{\mathrm{a}}(z) = c_{\mathrm{a}}^* T_{\mathrm{func}}(z), \quad (13)$$

where

$$T_{\mathrm{func}}(z) = \mathrm{e}^{(0.0967(T(z)-25))}, \quad (14)$$

where $T(z)$ is water temperature in °C at depth (z). The temperature function ($T_{\mathrm{func}}(z)$) is obtained from Christian and Karl (1995). The value used for remineralization rate of detrital nitrogen at 25 °C, c_{a}^*, is given in Table 3.

The state equation governing phosphate dynamics is of the form

$$\frac{\partial \mathrm{PO}_4^{3-}}{\partial t} = -\sum_{i=1}^{3} \rho_{\mathrm{PO}_4^{3-}i} + c_{\mathrm{p}}\mathrm{DOP}. \quad (15)$$

The only biological loss term for phosphate is uptake by each phytoplankton algal group, biological gain term is remineralization of DOP. This rate, $c_{\mathrm{p}}(z)$, is assumed to be modified by temperature, $c_{\mathrm{p}}(z) = c_{\mathrm{p}}^* T_{\mathrm{func}}(z)$, where c_{p}^* is given in Table 3. Aerosol N:P is universally very high and aerosol is always deficient in P relative to phytoplankton requirement (Baker et al., 2003). Aerosol molar N:P observed over the North Atlantic was 10^3–10^4 (Baker et al., 2003), therefore P deposition is not considered in this study.

The state equation of silicate, which is only used by algal group 3, the diatoms, is of the form

$$\frac{\partial \mathrm{Si}}{\partial t} = -\rho_{\mathrm{Si}_3} + c_{\mathrm{Si}}\mathrm{De}_l\mathrm{Si}. \quad (16)$$

The loss term for silicate is via uptake by algal group 3 only, as represented by the first term on the right side of Eq. (16). The gain term is dissolution of large detritus silicon ($c_{\mathrm{Si}}\mathrm{De}_l\mathrm{Si}$) (Nelson et al., 1995). Dissolution rate of detrital silicon, $c_{\mathrm{Si}}(z)$, is assumed to follow the temperature function given by Eq. (13).

2.4. DOM state equations

The DOM is partitioned into two components, non-refractory DON and DOP. These compartments are assumed to include both the semi-labile and labile pools. A DOC pool is not tracked explicitly in the current lower trophic level model, because carbon is not considered as a potentially limiting nutrient. Carbon losses in the state equations, e.g. by excretion (e.g. Eq. (9)), however, accounted for as gain terms to an implicit DOC pool.

The DON and DOP equations are very similar to each other, the only difference being that half (0.5) of the zooplankton excretion joins the DON pool, whereas all the excreted phosphorus enters the DOP pool. Thus only the basic state equation governing DON dynamics is given here, which is of the form

$$\frac{\partial \mathrm{DON}}{\partial t} = 0.5e_s Z_s \left(\frac{\mathrm{N}}{\mathrm{C}}\right)_{Z_s} + 0.5e_l Z_l \left(\frac{\mathrm{N}}{\mathrm{C}}\right)_{Z_l} + c_{\mathrm{DON}}\mathrm{De}_s + c_{\mathrm{DON}}\mathrm{De}_l - c_{\mathrm{a}}\mathrm{DON}. \quad (17)$$

The biological processes represented by the terms on the right side of Eq. (17) are excretion by microzooplankton, excretion by mesozooplankton, remineralization of small detrital nitrogen ($c_{\mathrm{DON}}\mathrm{De}_s$), remineralization of large detrital nitrogen ($c_{\mathrm{DON}}\mathrm{De}_l$), and remineralization of DON, respectively. The particulate carbon pools of each zooplankton group are converted to a nitrogen equivalent using a nitrogen to carbon ratio (N/C) for each group to estimate the amount of nitrogen in the excretion. Migrating zooplankton in the Sargasso Sea excrete 1–6% of body N daily in the

form of DON (Steinberg et al., 2000, 2002). Less is known about the microzooplankton release of DON; however, it is documented that ~5% of the nitrogen ingested by microzooplankton is released as dissolved free amino acids (Andersson et al., 1985; Nagata and Kirchman, 1991; Ferrier-Pages et al., 1998). Therefore the DON excretion is taken as $0.05\,d^{-1}$ for both micro and mesozooplankton in this study (Table 3).

DON and DOP sinks in the form of heterotrophic bacterial uptake are well documented (Bronk, 2002; Carlson, 2002; Karl and Bjorkman, 2002). It is shown that most of this uptake is converted to ammonium and phosphate, respectively, which can be used by phytoplankton (Bronk, 2002). The bacterial uptake of DON and DOP and its impact on bacterial biomass are not explicitly included in the model. The biogeochemical impact of heterotrophic bacteria are, however, assumed to be parameterized via the remineralization term (last term on the right side of Eq. (17)). The possible implications of the missing bacteria compartment on the modeled DON and DOP concentrations are further discussed in Section 5.1.

2.5. Detritus state equations

The governing equation for small detrital carbon (De_s) is assumed to be of the form

$$\frac{\partial De_s}{\partial t} + (w + sc_{des})\frac{\partial De_s}{\partial z} - \frac{\partial}{\partial z}K_z\frac{\partial De_s}{\partial z} = \sum_{i=1}^{3}[m_i P_i + (1-\lambda^*)I_{P_i}Z_s] + m_{Z_s}Z_s + (1-\lambda^*)(I_{P_3} + I_{Z_s})Z_l + m_{Z_l}Z_l - c_c De_s - aggDe_s, \quad (18)$$

where the three terms on the left side represent physical processes. Sinking of the small detritus pool (sc_{des}) is assumed to occur at a constant rate. The right side of Eq. (18) represents the biological processes that provide sources and sinks of De_s, which includes a source term through the death and unassimilated grazed fraction of algal groups, mortality of microzooplankton, unassimilated fraction of microzooplankton biomass that are grazed by mesozooplankton, and mortality (m_{Z_l}) by mesozooplankton, a loss term as aggregation (agg) to larger faster sinking detritus, De_l, and a loss term due to remineralization of De_s, respectively. Remineralization of small detritus carbon, c_c, is assumed to be modified by temperature and is given by an equation similar to Eq. (13). The definitions, values, and units of the parameters used in the De_s equations are given in Table 3.

The equation governing the large detrital carbon (De_l) dynamics is of the form

$$\frac{\partial De_l}{\partial t} + (w + sc_{del})\frac{\partial De_l}{\partial z} - \frac{\partial}{\partial z}K_z\frac{\partial De_l}{\partial z} = aggDe_s - c_c De_l, \quad (19)$$

where increases in large detrital carbon are supported by aggregation of small, slow sinking detritus and loss from the large detrital carbon occurs via remineralization (c_c) which is assumed to occur in a similar manner to small detrital carbon. The state equations for detrital nitrogen, phosphorus, and silicon are similar to Eqs. (18) and (19).

2.6. Model implementation

2.6.1. Numerical methods

The model domain extends from the sea surface to 200 m, which is below the 0.1% light level. This is sufficiently deep to include the total phytoplankton production in the upper waters of the Sargasso Sea. The system of equations describing the physical and biological dynamics of the state equations was solved numerically using a Crank–Nicholson scheme (Crank, 1956). This numerical integration scheme is unconditionally stable for the parameter ranges used in this study. The vertical coordinate was represented at 1 m intervals. A 1 h interval was used for the time integration, which allows resolution of the diurnal periodicity in phytoplankton growth kinetics. The model was run for 6 years with repeating forcing for year 1998, which was found to be sufficient to obtain a repeating seasonal cycle.

2.6.2. Surface and bottom boundary conditions

Surface boundary conditions were specified as no flux conditions (i.e. Neumann conditions) for all model state variables except for nitrate. For nitrate, the daily atmospheric flux and nitrogen fixation values in $\mu mol\,m^{-2}\,d^{-1}$ were used to specify an input. It was assumed that the nitrogen is deposited into the top $\Delta z = 1$ m grid box from where it is rapidly mixed over the surface mixed layer by the action of diffusion.

The bottom boundary conditions for nitrate, phosphate, silicate, and non-refractory DON were obtained from the BATS data and linearly interpolated to 1 h time intervals. Deep water DON,

which has limited bioavailability and reactivity, is assumed to represent the refractory organic nitrogen pool (Mahaffey et al., 2004) which is taken to be $2\,\mu mol\,N\,l^{-1}$ in this study. Bottom boundary conditions for DOP were obtained by assuming a DON:DOP ratio of $60\,mol\,mol^{-1}$ (Cavender-Bares et al., 2001; Ammerman et al., 2003). An observed minimum value at 150 m ($0.02\,\mu mol\,l^{-1}$, Lipschultz, 2001) is used to set the ammonium bottom boundary conditions at 200 m. The Neumann boundary condition, $\delta X/\delta z = 0$, is applied for phytoplankton and zooplankton compartments, also large diatoms, and small and large detritus are allowed to sink out of the bottom boundary.

2.6.3. Initial vertical profiles

Initial profiles of phytoplankton, zooplankton, nitrate, phosphate, silicate, DON, and detritus were obtained from the BATS data and linearly interpolated to 1-m depth intervals. Particulate organic carbon (POC) measurements are used to set the initial detrital carbon components by equally sharing the total POC between small and large components. Detrital nitrogen and phosphorus components are obtained from the detrital carbon values using the Redfield ratio (106 C:16 N:1 P). Only the non-refractory part of total DON is used by subtracting the refractory part. The phytoplankton biomass obtained from the BATS data were partitioned into three algal groups based on the relative ratios of these algal groups measured during other periods (Gin et al., 1999; DuRand et al., 2001). Initial profiles for DOP were obtained by assuming a DON:DOP ratio of $60\,mol\,mol^{-1}$ (Cavender-Bares et al., 2001; Ammerman et al., 2003). A constant average value of $0.03\,\mu mol\,l^{-1}$ (Lipschultz, 2001) is used to set the ammonium initial profile. Very small ($0.0001\,\mu mol\,C\,l^{-1}$) threshold values were set for the phytoplankton and zooplankton state variables, so that these concentrations do not become zero. This provides a refuge for these ecosystem components so they can respond when conditions become favorable for growth.

2.6.4. Nutrient and light limitation conditions

Nutrient uptake is calculated separately from carbon growth and all nutrients taken up by phytoplankton are added to the particulate nutrient pool of each algal group (cf. Section 2.1). During light limitation, the nutrient uptake rate can greatly exceed that of the light-limited carbon growth rate. Nutrient uptake continues over 24 h and is subject to the minimum carbon to nutrient ratios. The minimum carbon to nutrient ratios of each algal group and for each limiting nutrient are given in Table 2 in the form of maximum nutrient to carbon ratios (e.g. $Q_{N_{max}}$ for nitrogen to carbon ratio).

Light begins to inhibit algal group 1 at $48\,\mu mol\,quanta\,m^{-2}\,s^{-1}$ and inhibition is assumed to exponentially reduce the growth rate (Moore et al., 1995). This value is estimated by averaging the observed values for *Prochlorococcus* and *Synechococcus*.

3. Data

The biogeochemical data available from the BATS field studies provide measurements of many of the variables included in the lower trophic level ecosystem model. These measurements are used for comparison with the simulated distributions for specific days and depths, as well as for comparisons using a statistical analysis method (i.e. the Taylor (2001) diagram).

3.1. Advection, mixing, diffusion, and light

Bimonthly vertical advection values are taken from the Mercator North Atlantic circulation model which is based on OPA8.1 (Charria et al., 2006) and interpolated to hourly values. The effects of the mixing and diffusion are included in the ecosystem model using the temperature and salinity time-series from the BATS cruises. Time-varying mixed layer depth is taken to be the depth at which the change in σ_t over 1 m depth exceeds $0.05\,kg\,m^{-3}$. The vertical diffusion coefficient is set to $100\,cm^2\,s^{-1}$ in the mixed layer. Below the mixed layer it is set to $1\,cm^2\,s^{-1}$ to parameterize turbulent transport in the upper thermocline. This value is about an order of magnitude higher than the values observed by Ledwell et al. (1998); however, similar modeling studies (e.g. Hood et al., 2001; Dadou et al., 2004) show that using values given by Ledwell et al. (1998) results in considerable underestimation of nutrient concentrations. Hood et al. (2001) point out that high K_v values are roughly consistent with values inferred by Jenkins (1988) which possibly reflects the influence of isopycnal and mesoscale processes. Scale analysis shows that the modeled vertical advection of nutrients are an order of magnitude smaller than the vertical diffusion rates, possibly due to the underrepresentation of the mesoscale

processes in the three-dimensional model (Charria et al., 2006). Via the intense mixing in the surface mixed layer, all of the model compartments are always almost homogeneously distributed over the mixed layer. Sensitivity studies showed that setting the nutrients to observed values at the bottom boundary (cf. Section 2.6.2) and allowing them to get homogeneously mixed in the mixed layer results in sufficient entrainment of nutrients into the euphotic zone even when the mixed layer depth reaches 200 m (cf. Section 4.1).

The simulated surface light field, which provides input to the underwater light field, is obtained from a clear sky spectral irradiance model (Gregg and Carder, 1990) that is corrected for cloud cover effects using the shortwave radiation data obtained from Kallberg et al. (2004). Here, the non-spectral version of the bio-optical model described in Salihoglu (2005) is used. The light attenuation is represented as a function of the absorption and backscattering of sea water and particulate material. The pigment concentrations estimated for each algal group in the phytoplankton model are used to estimate particulate material concentration as a feedback into the bio-optical model. Details of the irradiance model and estimations of the algal pigment concentrations are given in Salihoglu (2005) and will not be described here.

3.2. In situ observations

The data sets used for calibration and evaluation (Section 4.1) of the simulations obtained from the lower trophic level ecosystem model were obtained from the BATS cruises (Steinberg et al., 2001). The data sets are from bimonthly process-oriented survey cruises and they were obtained via the BATS study web page (http://bats.bios.edu/). They include chlorophyll *a*, primary production, macronutrients, DON, POC, microzooplankton in the upper 200 m, and carbon fluxes at 200 m. High performance liquid chromatography (HPLC) determined indicator pigments were used to estimate cyanobacteria- and diatom-specific chlorophyll biomass using the equations of Anderson et al. (1996) which have been vetted in the Sargasso Sea. Eukaryotic autotrophs are estimated as the difference between total HPLC-derived chlorophyll *a* and contributions attributed to cyanobacteria and diatoms. Nutrient concentrations are converted from $\mu mol\,kg^{-1}$ to $\mu mol\,l^{-1}$ by using a conversion factor of $1.025\,kg\,l^{-1}$. Distribution of nitrogen fixation is also based on the observed values which are obtained from Orcutt et al. (2001) and Hansell et al. (2004).

4. Results

The ecosystem model described in the previous section was first used to establish a reference simulation that provides the basis for comparisons with other simulations designed to test model sensitivity to variations in processes and parameter values. The reference simulation is for 1 year, 1998, and for the BATS site at 31°40′N, 64°10′W. Year 1998 corresponds to a time period when zooplankton and DOP data are available together with the regularly collected biochemical data as described in Section 3.2. The observations from the BATS cruises allow evaluation of the results obtained from the reference simulation. The NAO is the dominant mode of atmospheric variability in the region (Hurrell et al., 2003), and the wintertime NAO was in its positive phase during 1998. This leads to reduced winter mixed layer depths and reduced associated nutrient supply (Oschlies, 2001).

4.1. Model evaluation

The simulated chlorophyll *a* concentrations in the water column (200 m) are close to the observations (Figs. 2a and b). Observations indicate that during the onset of the spring bloom (YD1–YD90) chlorophyll *a* concentrations were higher in the surface 50 m compared to the rest of the year. The model reproduces this difference in the chlorophyll *a* concentrations as well as the location and magnitude of the deep chlorophyll maxima (i.e. ~85 m, $0.4\,\mu g\,l^{-1}$). The chlorophyll *a* concentrations observed in the surface and between 110 and 130 m are underestimated by the model (Figs. 2a and b).

The observed chlorophyll *a* distribution patterns of the individual algal groups also support model results (Figs. 3a–f). The main discrepancies between the modeled and observed fields are the higher than observed algal group 1 chlorophyll *a* concentrations in the surface waters (Figs. 3a vs d) and higher modeled algal group 3 concentrations below the mixed layer (Figs. 3c vs f). Both model and observations suggest that the spring bloom is driven mainly by the autotrophic eukaryotes group (Figs. 3b and e). One interesting result is that both model and observations show that the chlorophyll biomass of cyanobacteria and diatoms are very low during the spring bloom period. Model results

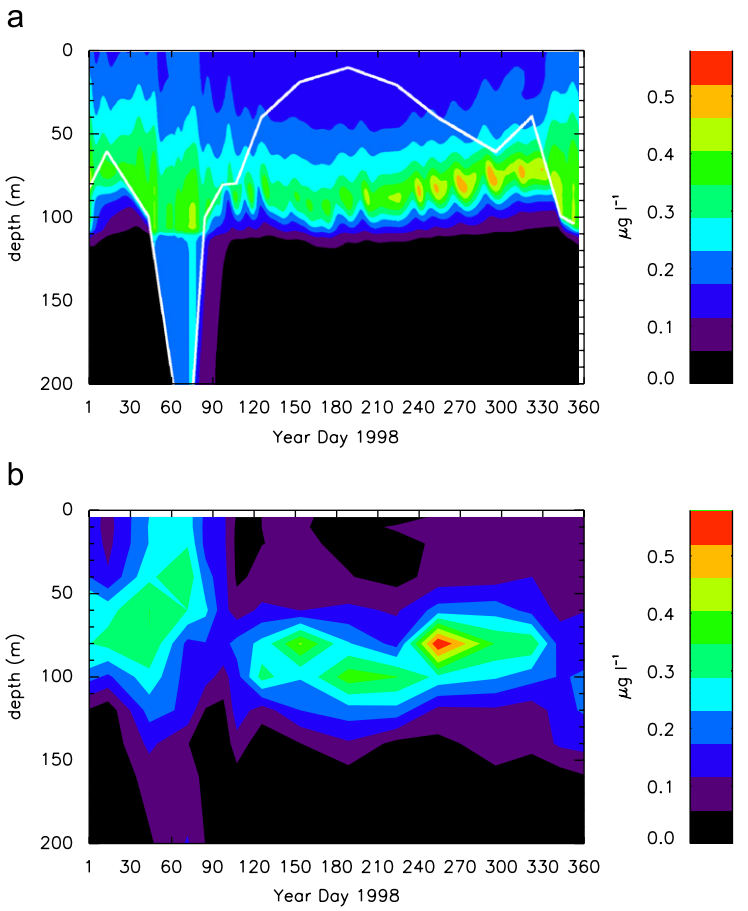

Fig. 2. Depth–time distribution of daily-averaged chlorophyll *a* ($\mu g\,l^{-1}$) obtained from (a) the reference simulation as the sum of all three algal groups (b) measurements during the BATS cruises. Overlaid solid white line in panel (a) represents the mixed layer depth.

suggest that all groups contribute to the deep chlorophyll maximum (DCM) during the oligotrophic summer period, when the contributions by autotrophic eukaryotes and cyanobacteria groups are the highest. Toward the end of the oligotrophic period, increase in the diatom chlorophyll *a* concentration is higher than observed (Figs. 3c and f). During this period, combination of low mesozooplankton abundance and a shallower nutricline with favorable light conditions results in net diatom growth.

There are no direct measurements of carbon biomass distribution of individual algal groups during year 1998. Analyses at BATS for years 1990–1994 (DuRand et al., 2001) show that eukaryotic phytoplankton dominate the phytoplankton carbon biomass. According to this analysis, the average phytoplankton carbon biomass at BATS is around 0.5 μmol C l^{-1} of which autotrophic eukaryotes constitute 35–73%, followed by cyanobacteria (i.e. *Prochlorococcus* and *Synechococcus*) with 20–58% and microphytoplankton (5%). Model results (Fig. 4) agree with the average phytoplankton biomass and species composition. It is interesting to see that the observed phytoplankton cell counts and carbon biomass estimations during 1992–1993 are relatively high in the surface waters during the whole year (DuRand et al., 2001), whereas chlorophyll concentrations (Steinberg et al., 2001) are very low, especially during summer, suggesting a very high carbon to chlorophyll ratio of surface phytoplankton. To test this, we have compared the surface observed POC values with simulated POC values. Results showed that although the modeled POC values agree well with the data (average surface values were 2.8 vs 2.5 μmol l^{-1}, respectively), modeled chlorophyll values are higher than the observations especially during the oligotrophic period (Figs. 2a and b). Underestimated carbon to chlorophyll *a* ratios,

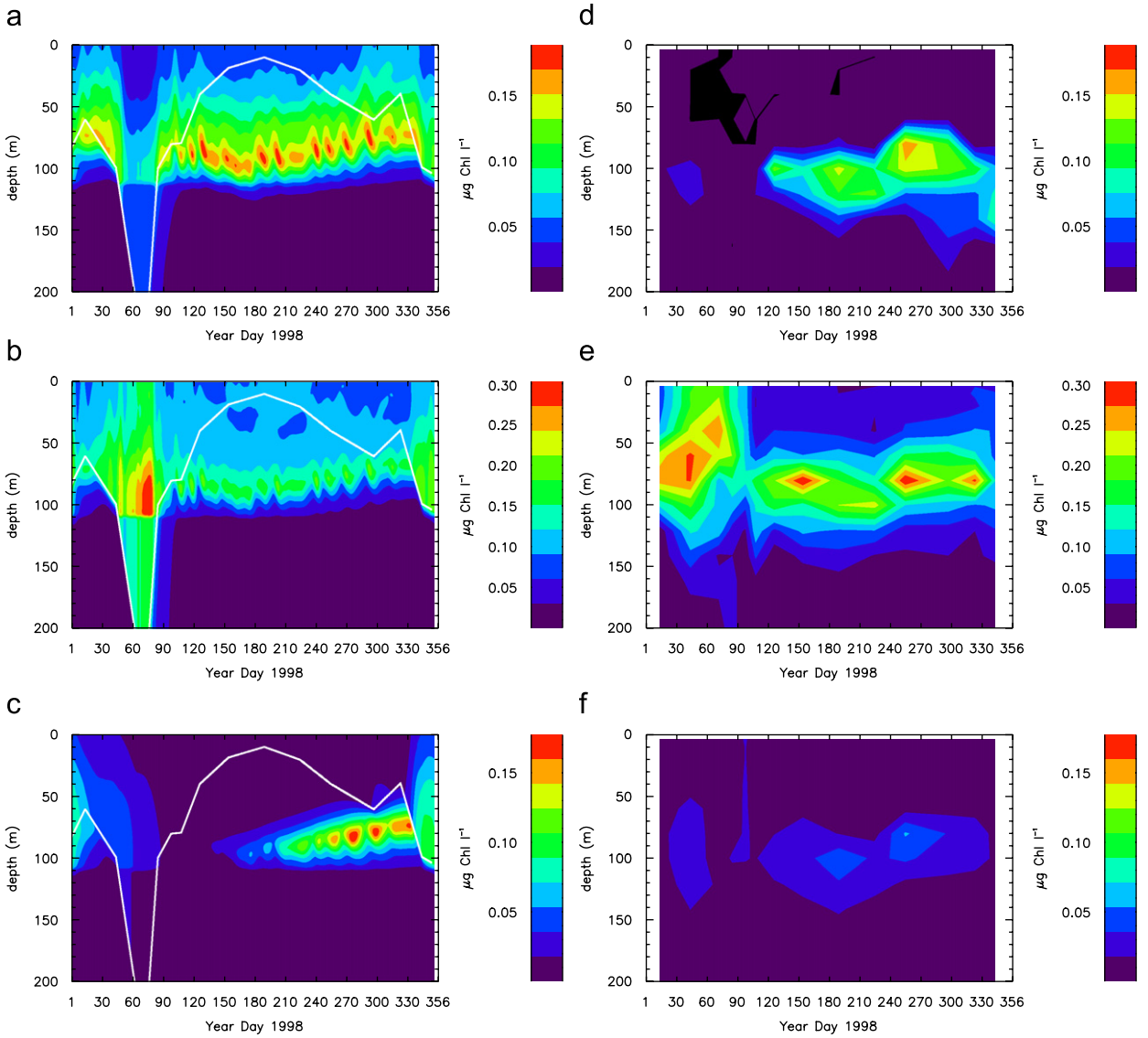

Fig. 3. Depth–time distribution of daily-averaged (a) cyanobacteria, (b) autotrophic eukaryotes, and (c) diatoms chlorophyll *a* ($\mu g\,l^{-1}$) concentration obtained from the reference simulation, and measured (d) cyanobacteria, (e) autotrophic eukaryotes, and (f) diatoms chlorophyll *a* ($\mu g\,l^{-1}$) concentrations during the BATS cruises. Overlaid solid white line in panels (a)–(c) represents the mixed layer depth.

which in the model were around 75, can be the reason for the model's overestimated surface chlorophyll *a* concentrations.

Simulated annually integrated primary production values ($11.2\,mol\,C\,m^{-2}\,yr^{-1}$) are identical to the primary production rates measured during the BATS cruises. The simulated maxima in primary production on YD30–YD80 and primary production values observed during the oligotrophic period, YD100–330, are comparable to the primary production rates measured during the BATS cruises (Figs. 5a and b). In particular, the vertical distribution of primary production, with relatively high surface values maintained even in summer, is simulated more realistically than by typical NPZD-type models, even when these are optimized to BATS data (e.g. Schartau and Oschlies, 2003b).

The simulated concentrations of nitrate, phosphate, and silicate are close to the observed ones (Figs. 6a, c, d vs 7a–c). However, the distribution of simulated nitrate and phosphate concentrations between ~120 and 200 m is more homogeneous (Figs. 6a and c) compared to the observations (Figs. 7a and b) because of smoothed fields in the

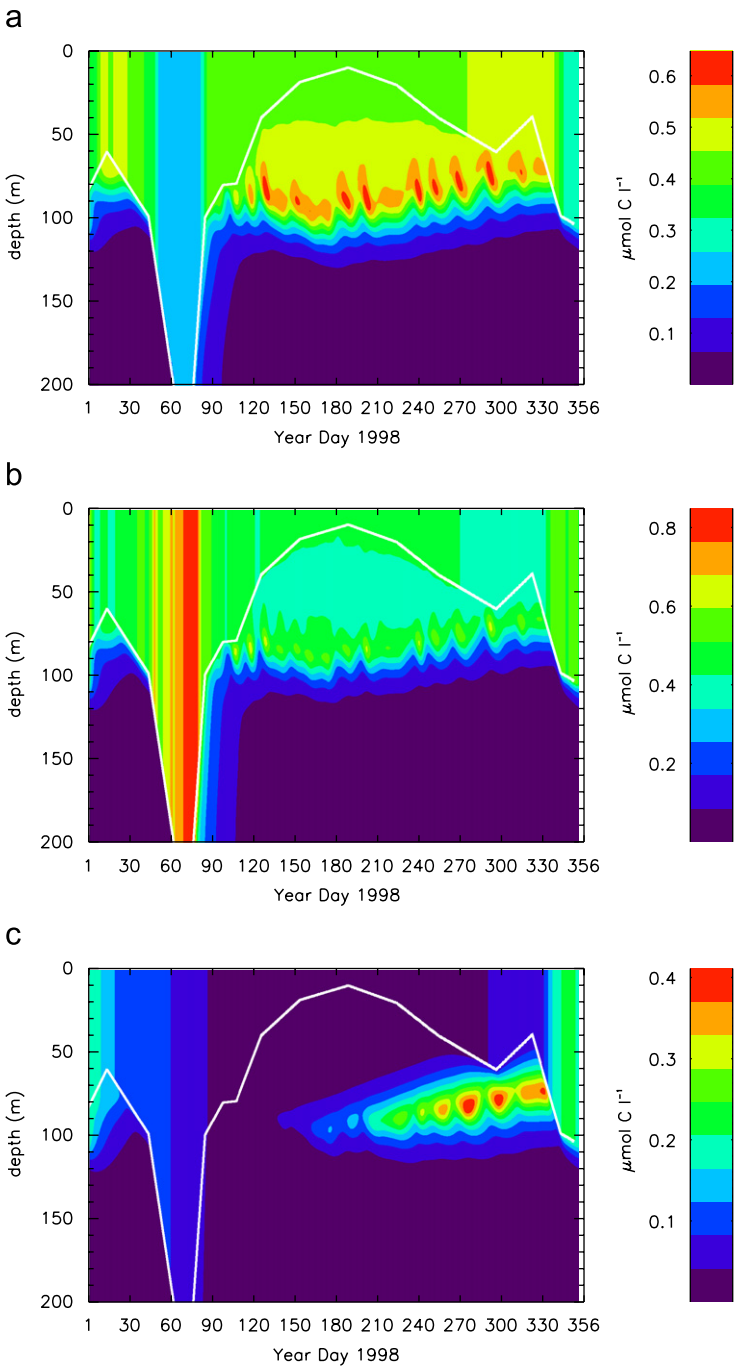

Fig. 4. Simulated depth–time distributions of algal biomass (μmol C l^{-1}) of (a) cyanobacteria, (b) autotrophic eukaryotes, and (c) diatoms.

physical dynamics (cf. Section 3.1). Modeled phosphate concentrations are completely depleted in the whole water column during YD50–YD90, whereas nitrate is still available (Figs. 6a and c), which is supported by the observations (Figs. 7a and b). Modeled phosphate concentrations also close to the measurements made at nanomolar level during March 1998 (Wu et al., 2000) indicating phosphate concentrations in surface waters near Bermuda were around 4 nM. There are no direct measurements of ammonium concentrations during 1998. Limited measurements (Lipschultz, 2001) indicate

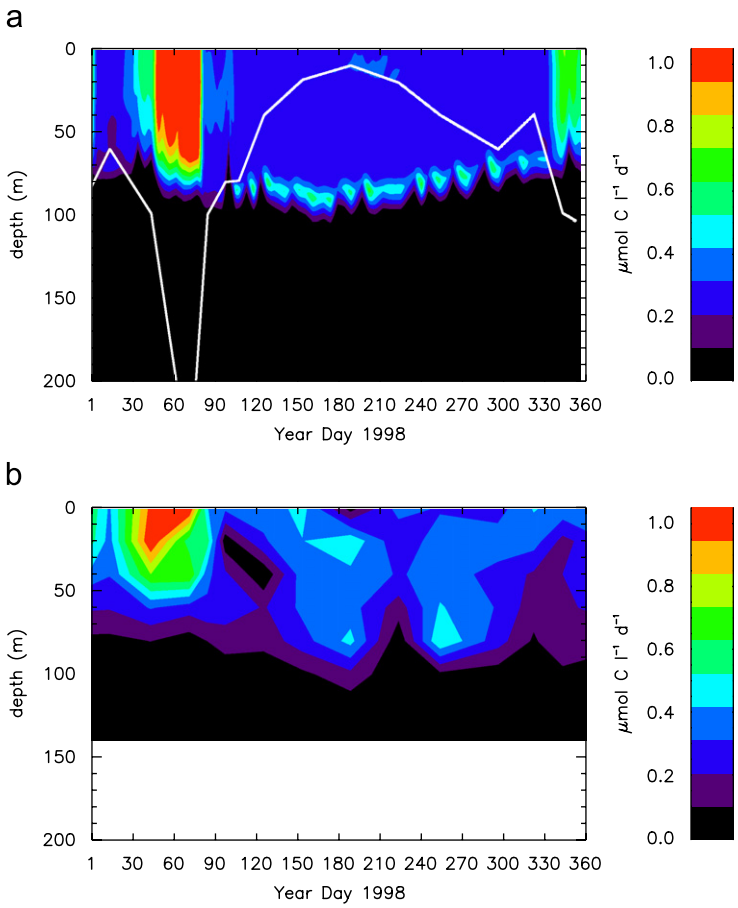

Fig. 5. Depth–time distribution of daily-averaged primary production (μmol C l^{-1} d^{-1}) obtained from (a) the reference simulation as the sum of the primary production of all three algal groups and (b) measurements during the BATS cruises.

that although subsurface maxima exist, the maximum concentrations are generally lower than 0.2 μmol N l^{-1}, whereas simulated subsurface values are in the 0.1−0.5 μmol N l^{-1} range (Fig. 6b). This discrepancy can be due to low ammonium uptake by autotrophic eukaryotes, because the abundance of this group is lower than observed after the spring bloom period (Figs. 3b and e). Long-term time-series of observations (Steinberg et al., 2001) show an average difference of ~20 m between the phosphocline and nitracline depths, with the phosphocline being systematically deeper. Our model results reproduce this difference, though the modeled phosphocline is merely ~10 m deeper than the nitracline (Figs. 6a and c).

Observed DON values are compared with the simulated values (Figs. 7d vs 6e) by subtracting the refractory part (2 μmol N l^{-1}, cf. Section 2.6.2). Observations show that DON concentrations increase from YD90–YD150 following the spring bloom. This increase is more pronounced and persistent in the simulation results (Fig. 6e). Although time-series of DOP data are not currently available, averaged DOP profiles observed for years 1995–1997 (Ammerman et al., 2003) indicate that model results (Fig. 6f) agree well with the annual averaged DOP values. Relatively few observations exist to evaluate the simulated zooplankton biomass and distribution (Madin et al., 2001). The simulated daily-mean vertically integrated zooplankton biomass is close to the observed values (385 vs 343 mg C m^{-2}, respectively). Night-time measurements of zooplankton biomass are used for the model–data comparison (Fig. 8a) assuming these values correspond better to the model results that do not account for the diurnal cycle of vertical zooplankton migration (Madin et al., 2001).

Although the available carbon flux measurements at 200 m can be subject to considerable experimental error (Dunne and Murray, 1999), the comparison of

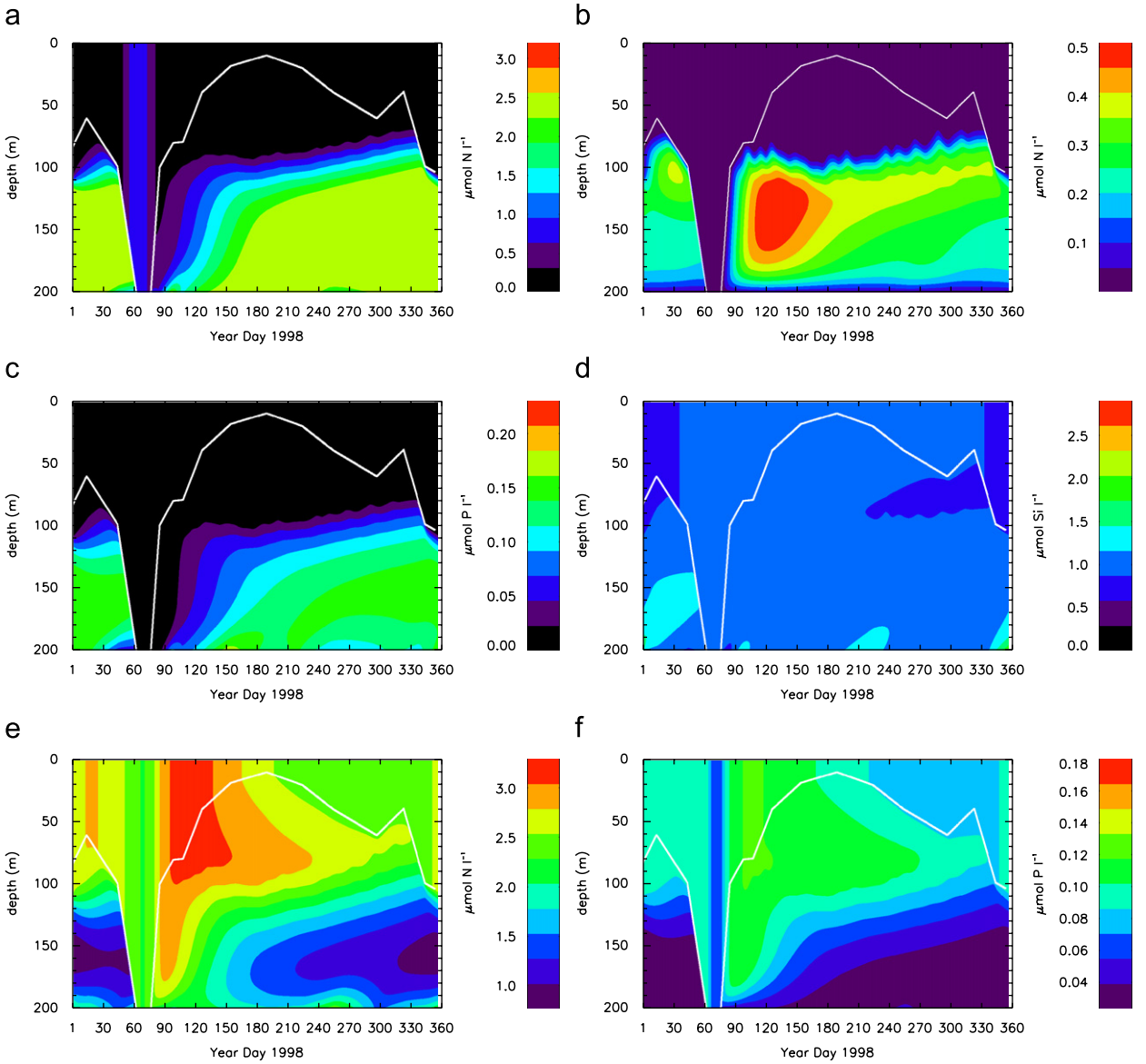

Fig. 6. Simulated depth–time distributions of concentrations of (a) nitrate (μmol N l^{-1}), (b) ammonium (μmol N l^{-1}), (c) phosphate (μmol P l^{-1}), (d) silicate (μmol Si l^{-1}), (e) DON (μmol N l^{-1}), and (f) DOP (μmol P l^{-1}).

the simulated organic particulate carbon flux to measurements is promising (Fig. 8b). The simulated fluxes overestimate the measured fluxes by 23% (921 mmol C m^{-2} yr^{-1} vs 708 mmol C m^{-2} yr^{-1}, respectively). Both simulated and observed organic particulate carbon fluxes show an increase in the late phase of the spring bloom period (Fig. 8b). A single measurement taken during the bloom period yields about half the model estimates. Climatological observations of carbon flux at 200 m (Steinberg et al., 2001) also indicate that carbon export during the bloom period can be lower than the simulated values.

Observed export ratios are calculated by dividing the 200 m sediment trap carbon fluxes by the water column integrated ^{14}C primary production rates (average of 0.071). The simulated export ratios are calculated similarly by dividing the downward 200 m carbon flux by the 200 m integrated primary production (Fig. 8c, blue line) and are close to the

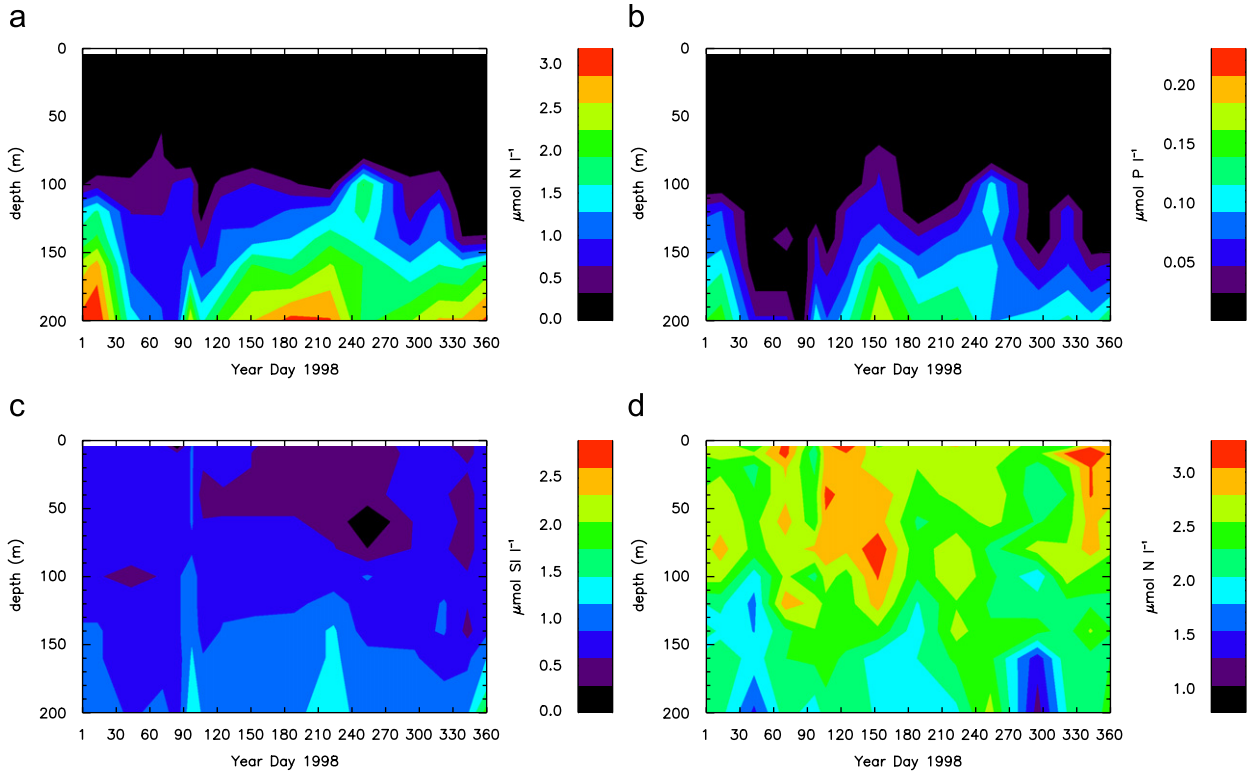

Fig. 7. Observed depth–time distributions of concentrations of (a) nitrate (μmol N l^{-1}), (b) phosphate (μmol P l^{-1}), (c) silicate (μmol Si l^{-1}), and (d) DON (μmol N l^{-1}) measured during the BATS cruises.

observations (average of 0.079). Modeled f-ratios, which are estimated by dividing nitrate uptake by total nitrogen uptake (nitrate + ammonium), are higher (average of 0.11, Fig. 8c, green line). Because nitrate assimilation rates are low and with nitrate largely derived from nitrification during the stratified summer period, which should therefore be considered recycled nitrogen (Lipschultz, 2001; Lipschultz et al., 2002), f-ratio values are estimated by removing nitrification from the model. These estimates show a high increase during the spring bloom (green line); however, estimates that are made using the carbon fluxes (blue line) show an increase following the spring bloom (Fig. 8c).

Model skill is further evaluated quantitatively using a Taylor (2001) diagram by comparing the total variance and space–time correlation between the model and the BATS data (Fig. 9). The model and observed standard deviation and correlation are computed for all the available data grid points (depth–time) during year 1998. A detailed description of the Taylor diagram and the statistics and computations involved are given in Taylor (2001) and will not be described here. The Taylor diagram indicates that model skill is highest for the depth–time distributions of nitrate and phosphate. Standard deviations of primary production, chlorophyll *a*, zooplankton biomass, and export ratios are low; however zooplankton biomass and export ratios show low correlation with the observations (cf. Section 5.1). Carbon flux and DON estimates show good correlation but low standard deviation values. Silicate skill evaluations show low correlation and high standard deviations.

4.2. Upper water column carbon budget

Analyses of the reference simulation results indicate that microzooplankton grazing of algal groups 1 and 2 ($\sim$29 mmol C m^{-2} d^{-1}) provides the primary pathway for carbon transfer between the primary and secondary producers (Fig. 10). Primary production by algal group 3 is low, and therefore removal by mesozooplankton also remains low.

The carbon transfer to the small detritus (Detritus1) compartment is mainly through the

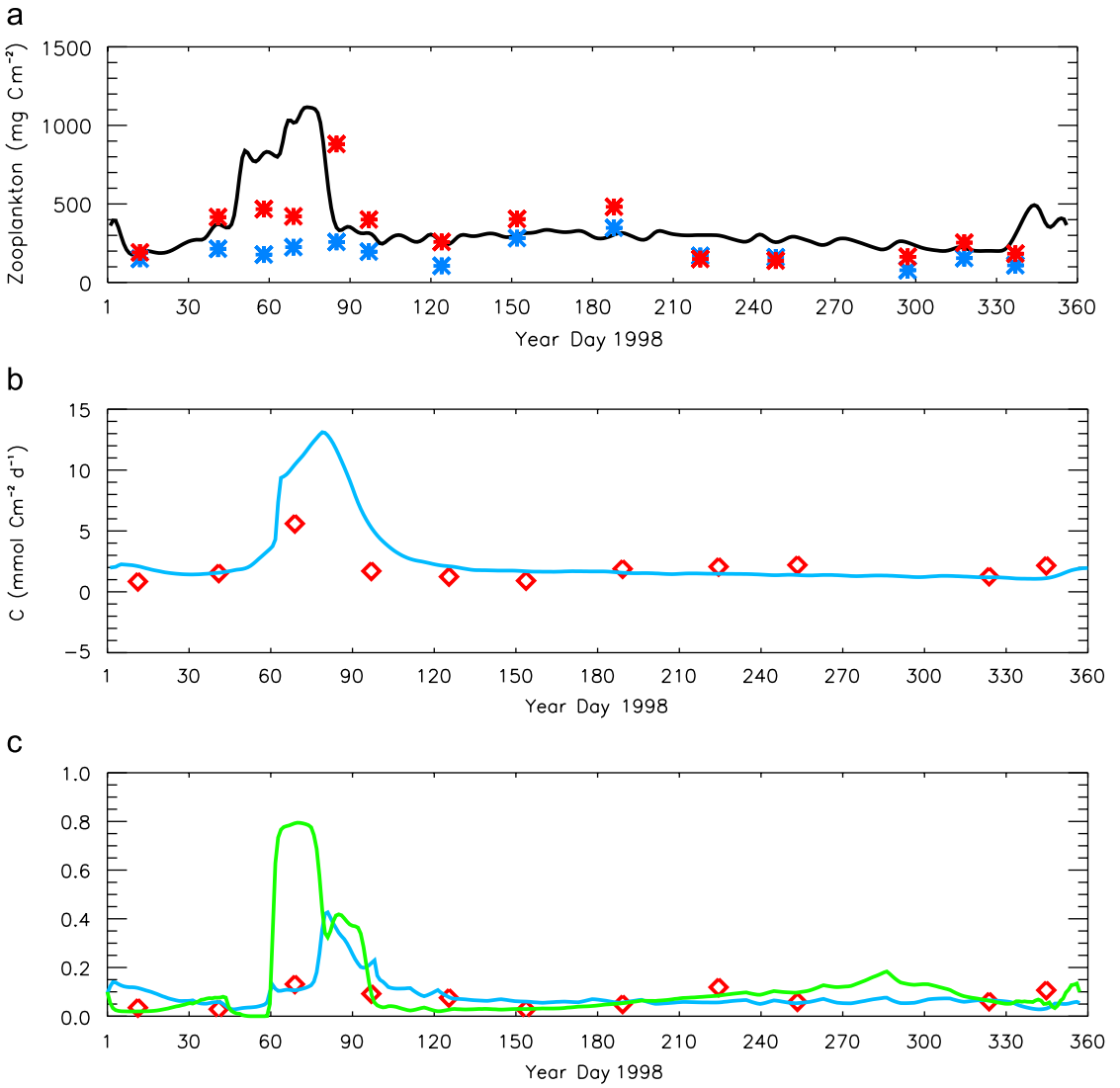

Fig. 8. Simulated time distributions of (a) zooplankton (mg C m^{-2}) integrated over the top 200 m. The corresponding zooplankton biomass measurements from the BATS cruises are shown with * for day-time (blue) and night-time (red) measurements, (b) carbon fluxes (mmol C m^{-2} d^{-1}) from 200 m, and (c) export ratios. Blue line denotes export ratios computed by dividing the downward carbon flux at 200 m by the 200 m integrated primary production and the green line shows 200 m integrated new nitrogen uptake to total (new + regenerated) nitrogen uptake ratio as *f*-ratio equivalent in panel (c). The carbon flux and export ratio measurements from the BATS cruises are indicated by the ⋄ symbols in panels (b) and (c), respectively.

unassimilated part of grazed phytoplankton and non-grazing mortality by algal groups 1 and 2 (14 mmol C m^{-2} d^{-1}) and microzooplankton death (12.5 mmol C m^{-2} d^{-1}). Removal of microzooplankton by mesozooplankton is modest (3.5 mmol C m^{-2} d^{-1}). Most of the small detritus is recycled in the upper water column (28 mmol C m^{-2} d^{-1}) and the rest is mainly aggregated to large, fast sinking detritus (Detritus2, 3.7 mmol C m^{-2} d^{-1}). The export of the latter detritus compartment is the main pathway of carbon transfer out of the upper water column (2.2 mmol C m^{-2} d^{-1}).

One interesting result is that the relative contributions of each algal group to total primary production and standing stock (biomass) are not proportional to each other. Most (63%) of the production is by algal group 2 and the biomass

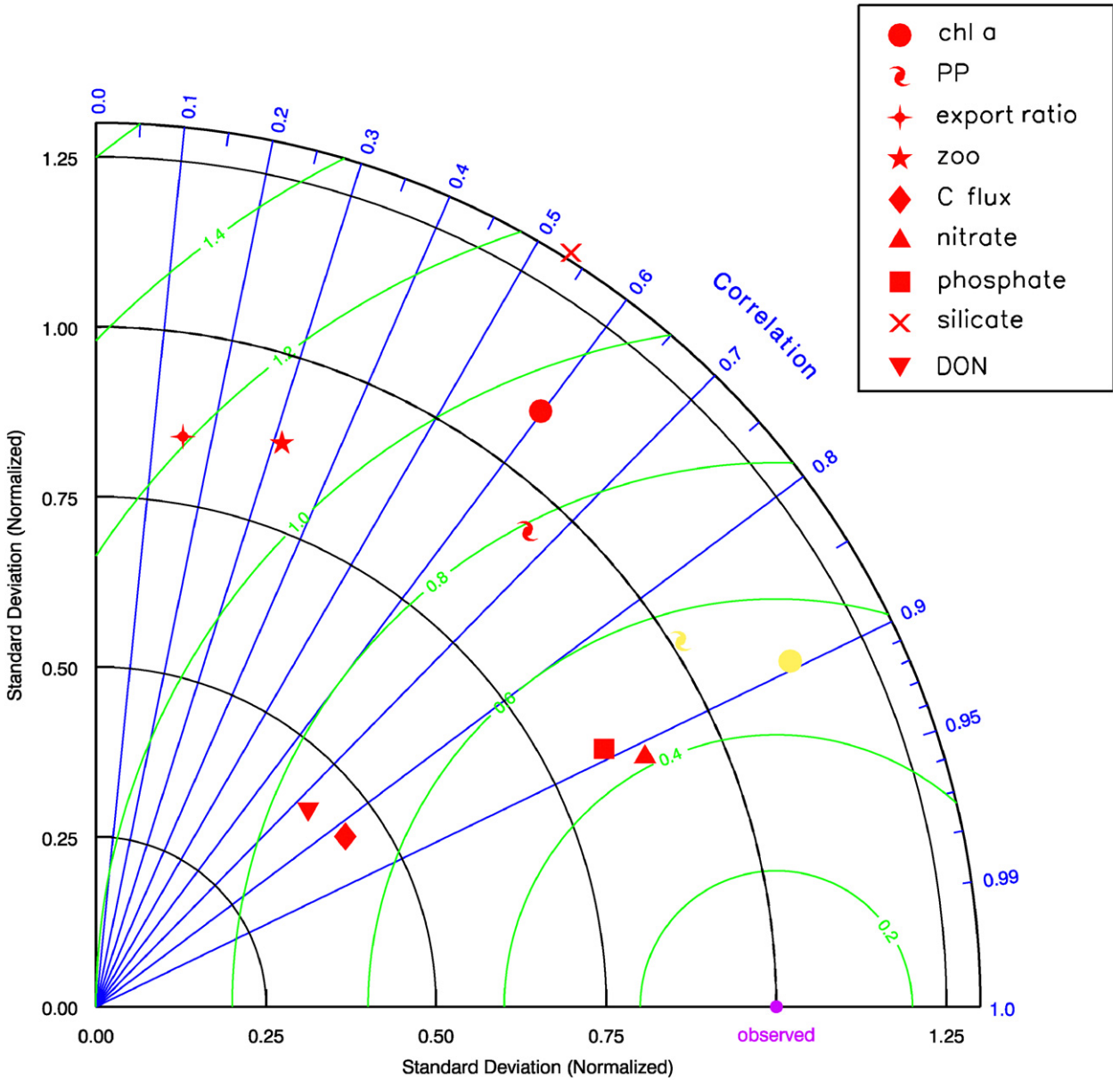

Fig. 9. Model performance analyses using the Taylor diagram. The radial distance from the origin is proportional to the standard deviation of a pattern. The centered root mean square difference between the model and data (observed) fields (green line) is proportional to their distance apart (normalized). The correlation between the two fields is given by the azimuthal position of the test field. Comparisons are done using the data in the whole water column (200 m). Yellow symbols show model skill evaluation done by considering water column averaged values. Abbreviations used are: chl *a*—chlorophyll *a*; PP—primary production; zoo—zooplankton biomass; C flux—carbon flux at 200 m; DON—non-refractory dissolved organic nitrogen.

of this group corresponds to 50% of the total biomass. However, although production by algal groups 1 and 3 are 33% and 3% of the total primary production, biomass of these groups amounts to 40% and 10% of the total biomass, respectively.

4.3. Influence of nitrogen fixation, atmospheric deposition, and deviations from the Redfield stoichiometry

As described in Section 2.3 nitrogen fixation and atmospheric nitrogen deposition are included using

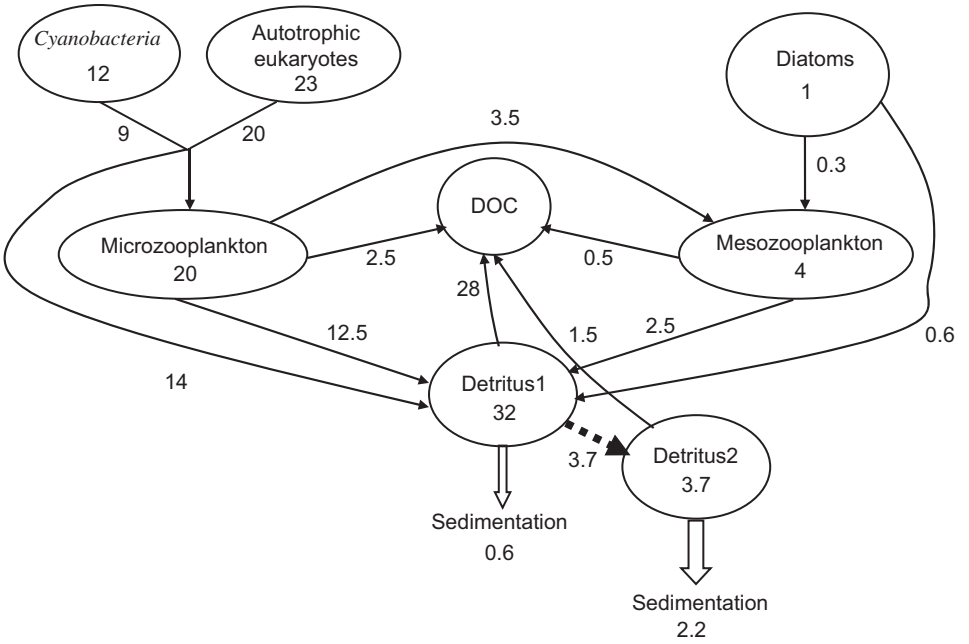

Fig. 10. Flowchart of the simulated carbon budget (mmol C m^{-2} d^{-1}) obtained for the lower trophic level model structure used in this study. Arrows indicate the direction of carbon transfer between model compartments in mmol C m^{-2} d^{-1}. The ecosystem variables are daily averaged over the euphotic zone (0–200 m). The numbers in the algal group, zooplankton, detritus, and dissolved organic carbon (DOC) compartments are the net daily gain values that are given in the state equations in Section 2. Arrows between algal groups and zooplankton compartments and the arrow between microzooplankton and mesozooplankton compartments indicate net daily grazing. Arrows between phytoplankton and small detritus (Detritus1) compartments are unassimilated part of grazed phytoplankton and phytoplankton non-grazing mortality. Arrows between zooplankton and Detritus1 and DOC indicate the carbon loss from zooplankton resulting from mortality and excretion, respectively. Dashed arrow between Detritus1 and large, fast sinking detritus (Detritus2) represents aggregation. Arrows between the detritus compartments and the dissolved organic carbon (DOC, which is not tracked in the model) indicate the loss of carbon from the detritus compartments by remineralization.

observed values (Orcutt et al., 2001; Baker et al., 2003; Hastings et al., 2003; Hansell et al., 2004). To understand the influence of these extra nitrogen inputs, sensitivity analyses are performed by removing the extra nitrogen inputs from the reference simulation. Results showed that the contribution of nitrogen fixation and deposition corresponds to 3.6% of annually integrated primary production and 12% of annual new production. Atmospheric nitrogen deposition corresponds to ~25% of these contributions (Table 4).To understand the influence of high geochemical nitrogen fixation estimates on the ecosystem dynamics, a sensitivity experiment employs the regional value estimated by Michaels et al. (1996) (0.23 mol N m^{-2} y^{-1}), which is around five times higher than the estimate by Hansell et al. (2004) (0.045 mol N m^{-2} y^{-1}). These results show a 5% increase in primary production compared to the reference run (Table 4). The share of nitrogen fixation on new production is increased from ~9% to ~25%. Whereas, when Orcutt et al.'s (2001) (0.015 mol N m^{-2} y^{-1}) estimates are used, results show a 2% decrease in primary production compared to the reference run.

Table 4
Annual integrated carbon biomass (total biomass, mmol C m^{-2} yr^{-1}), annual integrated primary production (total PP, mmol C m^{-2} yr^{-1}), and annual integrated new production (total NP, mmol C m^{-2} yr^{-1}) calculated from the reference simulation and modified simulations in which nitrogen (N) fixation is removed, nitrogen fixation values of Michaels et al. (1996) are used, dust deposition is removed, cellular nutrient ratios are set close to the Redfield ratio (cf. Section 4.3), and remineralization of nutrients is removed from the reference model

Simulation	Total biomass	Total PP	Total NP
Reference	40 122	11 200	2558
No N fixation	40 120	10 900	2328
High N fixation	40 207	11 847	2916
No dust deposition	40 120	11 100	2481
Redfield cell quotas	37 170	7399	2370
No remineralization	14 575	2558	2558

Recent literature shows that maximum N:C and P:C ratios are generally above the Redfield ratios and minimum N:C and P:C are below the Redfield ratios (Table 2). Observations also show that cyanobacterial cellular N:C ratios are higher (Bertilsson et al., 2003) compared to autotrophic eukaryotes and diatoms (Leonardos and Geider, 2004), whereas cellular P:C ratios show the opposite trend (cf. Section 2.1, Table 2). To understand the implications of this non-Redfield structure, sensitivity tests are performed by setting the phytoplankton intracellular N:C and P:C ratios close to the Redfield ratio. This is done by allowing the minimum and maximum N:C and P:C cellular ratios change in a narrow band (±10%) around the Redfield ratio.

This test run yielded the interesting result that the annual primary production decreases considerably (35%), whereas total phytoplankton biomass decreased by "only" 8%. Although the primary production of all groups decreased considerably, algal groups 3 and 2 were the most affected groups. The decrease in primary production was particularly pronounced during the oligotrophic period (Fig. 11). The biomass of algal groups 2 and 3 decreased strongly, whereas biomass of algal group 1 actually increased. The decrease in overall primary production resulted in the decrease of zooplankton biomass, and this decrease in top-down control most strongly affected the biomass of strongly grazer controlled algal group 1.

Restricting the cellular N:C and P:C quotas to values close to the Redfield ratio had a prominent effect on the distribution of nutrients (Figs. 12a–f). Unrealistic accumulation of nitrate and ammonium concentrations is seen in the surface waters (Figs. 12a and b), whereas phosphate concentrations decreased. The modifications in the cellular nutrient ratios resulted in an increase in phosphate uptake and decrease in nitrogen uptake, and a shift toward increased phosphorus limitation. Silicate concentration increased (Fig. 12d) because of high decrease in algal group 3 production. Decreased primary production led to decreased DON and DOP concentrations in the water column (Figs. 12e and f).

Using the Redfield nutrient cellular ratios has also considerable implications for the water column N:P ratio. Results of the reference model run show that the ambient nitrate to phosphate ratios were very high (~60) right above the nitracline and in the whole water column during YD60–YD100 (Fig. 13a). During the YD120–YD330 N:P ratios were ~8 in the upper 70 m and below 100 m they were ~25. Right on top of the nitracline a very sharp increase in nitrate to phosphate ratios occurs because the phosphocline is located deeper than the nitracline (cf. Figs. 6a and b). Although the total dissolved nitrogen to phosphorus (TDN:TDP) ratios show complex distribution patterns, simulations indicate that TDN:TDP ratios vary between 20 and 45 (Fig. 13b). When the Redfield cellular values were used ambient nitrate to phosphate and TDN:TDP ratios increased considerably in the upper 130 m (Figs. 13c and d).

4.4. Limiting nutrients

For decades marine biologists and geochemists have debated which nutrient (i.e. nitrogen or

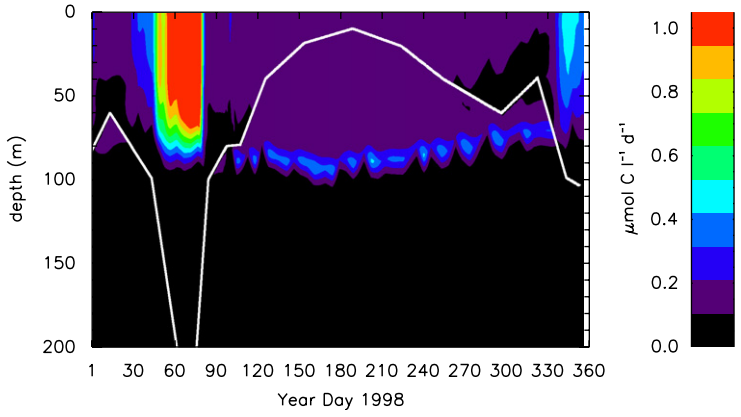

Fig. 11. Depth–time distribution of daily-averaged primary production (μmol C l^{-1} d^{-1}) obtained from the modified model run where the cellular nutrient ratios are set close to the Redfield ratio (cf. Section 4.3).

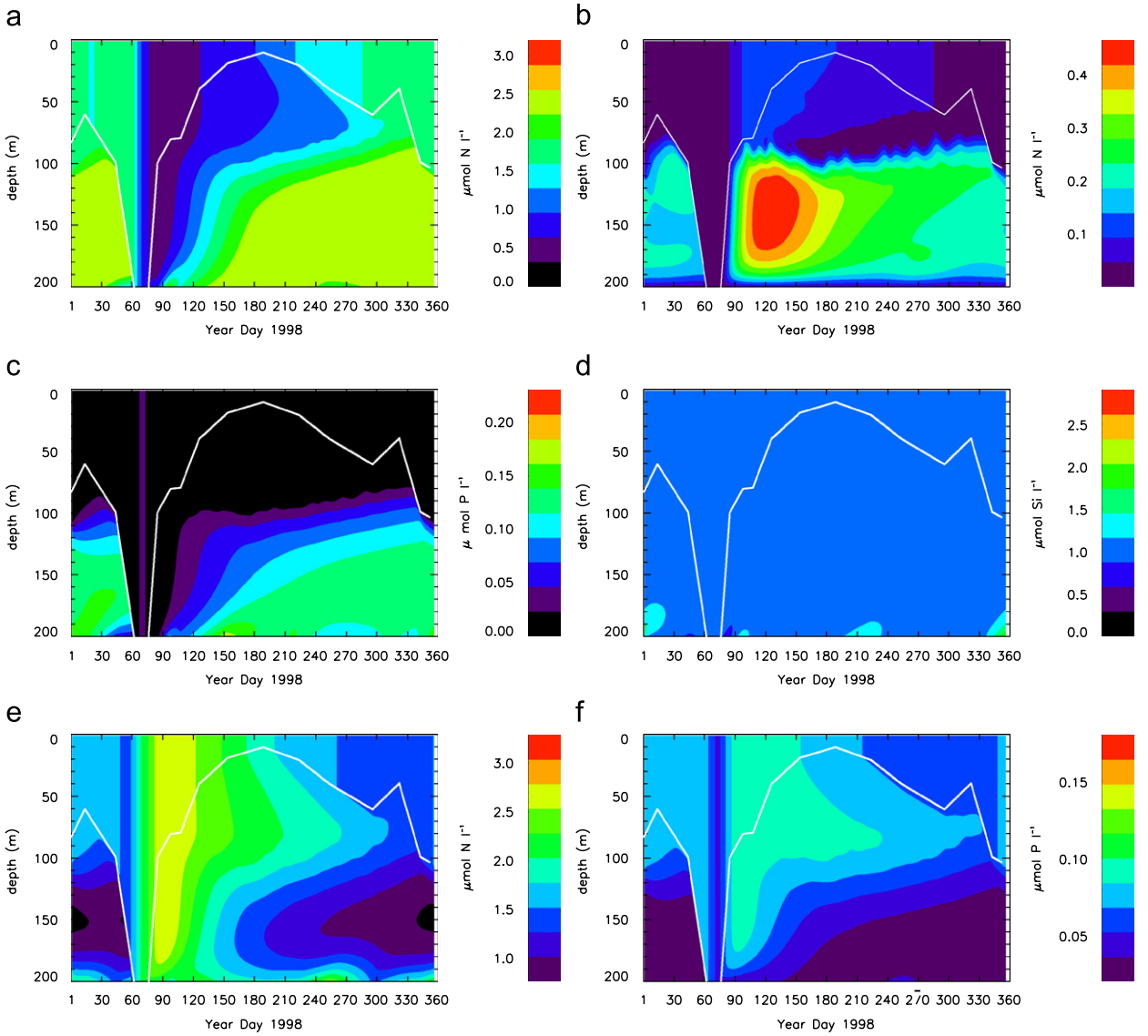

Fig. 12. Simulated depth–time distributions of concentrations of (a) nitrate (μmol N l^{-1}), (b) ammonium (μmol N l^{-1}), (c) phosphate (μmol P l^{-1}), (d) silicate (μmol Si l^{-1}), (e) DON (μmol N l^{-1}), and (f) DOP (μmol P l^{-1}) obtained from the modified model run where the cellular nutrient ratios are set close to the Redfield ratio (cf. Section 4.3).

phosphorus) limits marine phytoplankton growth. Inclusion of three nutrient groups in the model allows the assessment of limiting nutrients. Moreover, one big advantage of estimating the intracellular nutrient ratios is that these ratios are very good proxies of limiting nutrients. If the nutrient to carbon ratio is below its set maximum value this indicates that the algal group is limited by that nutrient.

Simulated nutrient distributions (Figs. 6a–c) show that nitrate, ammonium, and phosphate are depleted within the mixed layer and thereby potentially limit the growth of phytoplankton. Nitrate concentrations only show a peak during YD65–YD90 which is also reflected in the phytoplankton cellular N:C ratios (Figs. 14a–c). In general, cellular N:C ratios of all algal groups reach their maximum during periods of mixed layer deepening (YD1–YD15, YD35–YD90, YD340–YD360). Simulations indicate that nitrogen limitation is similar for all algal groups during the first 3 months of the year, whereas it is weaker for

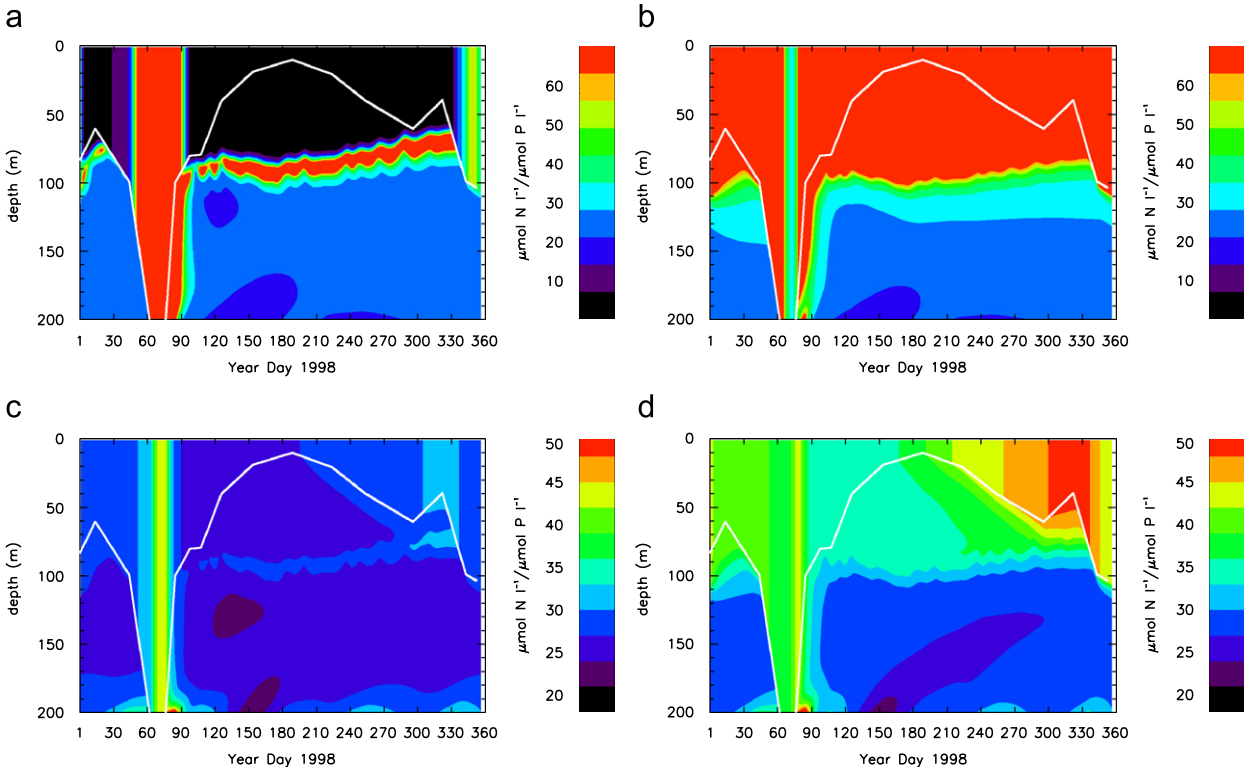

Fig. 13. Simulated depth–time distributions of (a) ambient nitrate to phosphate and (b) total dissolved nitrogen to phosphate (mol mol^{-1}) obtained from the reference simulation, and (c) ambient nitrate to phosphate and (d) total dissolved nitrogen to phosphate (mol mol^{-1}) obtained from the modified model run where the cellular nutrient ratios are set close to the Redfield ratio (cf. Section 4.3).

algal group 1 during the rest of the year. Nitrogen limitation is more pronounced for algal groups 2 and 3 during the oligotrophic period and nitrogen limitation extends below the mixed layer to ~70 m. Below ~70 m no nitrogen limitation occurs.

Different from nitrate, phosphate is always depleted in the mixed layer even during the deepening of the mixed layer during spring (Fig. 6c). However, cellular P:C ratios of algal groups 1 and 2 increase during the spring period (Figs. 14d and e). During the whole year, values of P:C ratios in the mixed layer for algal group 1 are below its maximum but generally well above its minimum values. This suggests moderate phosphate limitation for this group except for the period following the deepening of the mixed layer during YD60–YD80 where P:C ratios are close to their minimum values. Simulations suggest that algal groups 2 and 3 are strongly limited by phosphate (Figs. 14e and f). Phosphate limitation of algal group 2 is relieved during YD60–YD80 in the mixed layer; however, algal group 3 remains strongly phosphate limited during this period as well. These results show the model's capability to simulate the shifts in limiting nutrients among algal groups. Also, sensitivity studies have shown that nitrogen fixation is not the main reason for phosphate limitation as even in the absence of nitrogen fixation the ecosystem remains strongly phosphate limited.

Simulated silicate concentrations are around 1 µmol Si l^{-1} in the mixed layer (Fig. 6d) which corresponds to the half saturation constant of silicate uptake by algal group 3. Cellular Si:C concentrations (not shown) indicate that silicate can limit the growth of algal group 3 only during a short time period (YD210–YD330) at the depth of the DCM. These results suggest phosphorus and nitrogen limitations on diatoms (Figs. 14c and f) prevent severe depletion of silicate.

Results of sensitivity studies show that recycled nutrients are important components that drive the ecosystem (Table 4). All the remineralization terms (i.e. c^* terms) in the model are turned to zero to test the influence of nutrient recycling. Overall a ~75% decrease in primary production of algal groups occurred when the nutrient remineralization was

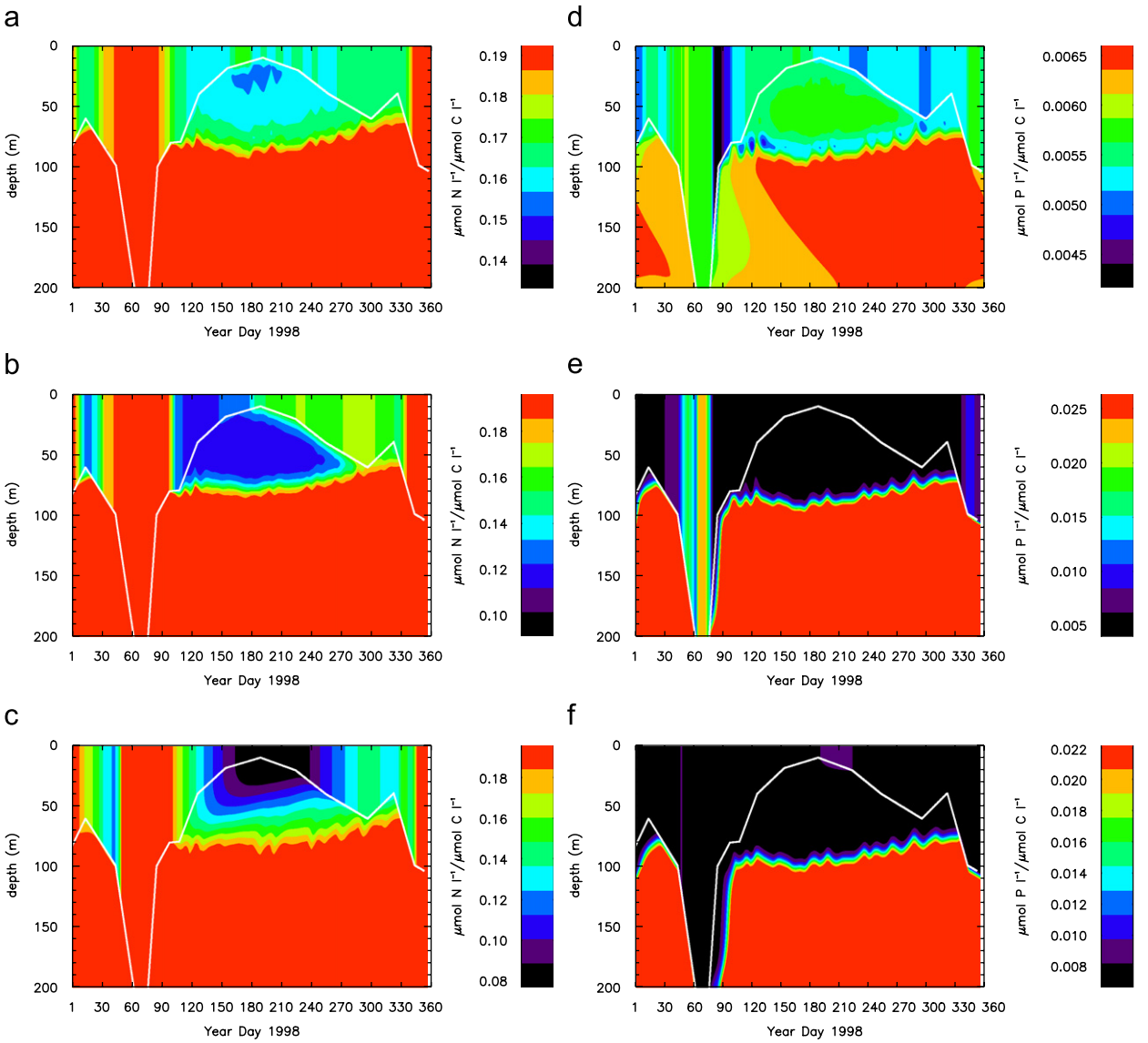

Fig. 14. Simulated depth–time distributions of phytoplankton cellular N:C ratios for (a) cyanobacteria, (b) autotrophic eukaryotes, (c) diatoms, and phytoplankton cellular P:C ratios for (d) cyanobacteria, (e) autotrophic eukaryotes, (f) diatoms. The contour plot ranges are scaled so the red colors indicate the maximum N:C and P:C ratios that are given in Table 2.

removed from the reference model. Results of the reference simulation show that relative contribution of recycled nutrients to primary production is much less (18%) during the bloom period, whereas it can increase up to 90% during the oligotrophic period.

5. Discussion

The modeling approach used in this study provides a framework for quantitatively testing the understanding of factors that control phytoplankton biomass, primary production, and export production at the BATS site in the Sargasso Sea. The simulated model state variables and cell quota ratios show the importance of nutrients dynamics and interactions between the algal groups in defining the composition of the phytoplankton community and carbon production and export.

5.1. Model performance

A wide range of biogeochemical provinces and diverse phytoplankton communities with distinct physiological differences introduce complexities to

marine ecosystem modeling. The ecosystem model presented in this study is an attempt to provide enough flexibility to represent biogeochemical processes in the Sargasso Sea. Here we will mainly focus on understanding the model skill by using a wide range of biogeochemical observations. It is complicated to do model–model comparisons because each model uses a different physical forcing field and biogeochemical formulations. Therefore, below we have attempted to discuss those differences identified in our model results that are due to including three algal groups and the phosphorus cycle. Most of the multi-component models developed for the region (e.g. Doney et al., 1996; Oschlies and Garçon, 1998; Spitz et al., 2001; Hood et al., 2001; Anderson and Pondaven, 2003; McGillicuddy et al., 2003; Schartau and Oschlies, 2003a; Dadou et al., 2004) assume fixed C:N:P ratios, most commonly the Redfield ratio of 106 C:16 N:1 P. Previous cell quota models (Bissett et al., 1999a; Mongin et al., 2003; Lima and Doney, 2004) mainly considered nitrogen and silicon as the limiting nutrients. The present study differs in that it combines carbon, nitrogen, phosphorus, and silicon cycles. Also DON and DOP compartments are explicitly included in this model (Fig. 1), whereas DOC is treated implicitly.

Our model shows better skill than many previous attempts in simulating the combination of observed spatial and temporal patterns in nutrients, chlorophyll, primary production, zooplankton, carbon export, and f-ratios. Schartau and Oschlies (2003a) showed that having one group of phytoplankton with constant growth parameters results in systematic model–data misfits in primary production and chlorophyll concentrations. Having three algal groups gives the model the flexibility to adapt to different environmental conditions through shifts in species composition (cf. Fig. 3). Also in an accompanying paper Schartau and Oschlies (2003b) showed the inadequacy of applying constant C:N ratios to convert simulated phytoplankton nitrogen uptake to carbon-based primary production results in errors in primary production patterns. Similar errors are documented by Anderson and Pondaven (2003), whose modeled export carbon fluxes significantly (more than twice) exceed sediment trap estimates. Although the reason for this misfit is not explained, our study shows that it is possible to reproduce carbon export values that are comparable with the sediment trap data while having realistic primary production and nutrient predictions (cf. Section 4.1). The study by Mongin et al. (2003) is perhaps the modeling study most comparable to ours. They also used the Droop equations to simulate phytoplankton nutrient uptake and growth dynamics. In their two phytoplankton group (i.e. picoplankton and diatoms) model they considered nitrogen and silicate limitations. Their modeled primary production and nutrient fields are in reasonable agreement with the observations. Having two phytoplankton groups in the model structure results in the overestimation of the diatom biomass. This type of discrepancy also occurred and was discussed in other modeling studies (e.g. Christian et al., 2002). However, the main difference between our model and that of Mongin et al. (2003) is the inclusion of the phosphorus cycle in our model. This aspect will be further discussed in Section 5.4.

Although direct comparisons between model and data give satisfactory results, skill assessment using the Taylor diagram produces a less convincing picture. For example, although the magnitude of observed and simulated export ratios match well, 0.079 vs 0.071, respectively (Fig. 8c), the Taylor diagram shows poor skill because of low correlation between the model and observed values. Observed export ratios are consistently low and the model cannot possibly capture small deviations about the mean. Even subtle physical processes and errors involved with data collection (Steinberg et al., 2001) can result in such scatter when observed values are continuously close to the noise level. When water column averaged values are considered, for example, for chlorophyll a and primary production, considerable improvement in correlation is seen (Fig. 9, yellow symbols). However, for the sake of a complete model skill assessment all the available data are used to consider the highest resolution observed variability in space (water column) and time.

An important discrepancy between model and observations is the too high simulated DON pool during the period that follows the spring bloom (Fig. 6e), mainly due to remineralization of particulate organic matter to DON. Although an increase in surface DON concentrations following the spring bloom is observed during year 1998 (Fig. 7d), a longer time-series of observed DON (Fig. 15) suggest that this is not an annual pattern. Thus, it is not clear whether this increase during 1998 is due to the spring bloom or not. However, the remineralization rates used in this study are also

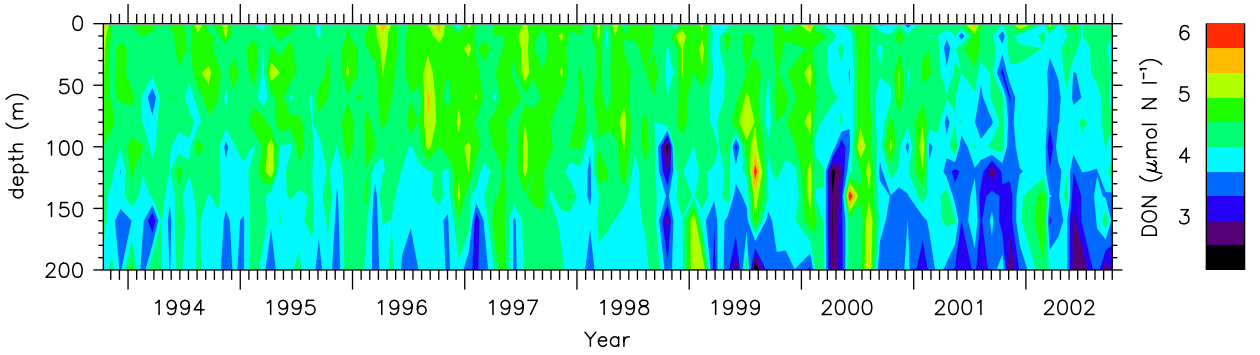

Fig. 15. Observed depth–time distribution of concentrations of DON (μmol N l^{-1}) measured during the BATS cruises.

suggested by the observations of Benitez-Nelson (2000), and DON remineralization at such rates is required by the model to correctly simulate primary production and carbon and nitrogen export. As Steinberg et al. (2001) showed, maximum bacterial abundance and production are observed during late spring, persist throughout the summer, and begin to erode in autumn, overlapping with the modeled DON cycle (Fig. 7d). Presumably more DON is taken up and tied up in bacterial biomass during this period; therefore the missing bacteria component in the model may help to explain this mismatch. This result may have implications on current modeling studies that include DON. Even the models that include bacteria compartments, which can take up DON, predict a strong annual DON cycle (e.g. Hood et al., 2001; Spitz et al., 2001; Anderson and Pondaven, 2003). This suggests that the remineralization or the uptake kinetics of DON (or both) are not represented correctly in the models and need to be re-evaluated as more observations become available.

5.2. *Phytoplankton community, carbon production, and export*

Model results show that the spring bloom is driven mainly by the autotrophic eukaryotes, and that during the oligotrophic period the cyanobacteria and microplankton communities are increasingly abundant at the depth of the deep chlorophyll maxima. This shows the model's capability to simulate observed shifts in species composition (DuRand et al., 2001; Steinberg et al., 2001) with respect to environmental factors. Observations support the model results (Figs. 3a–f) that eukaryotic phytoplankton is the most abundant group during the spring bloom and eukaryotic carbon contribution is almost always larger than that of picoplankton although during late summer and fall cyanobacteria biomass constitutes almost half of the phytoplankton biomass. Observations and model results are in consensus that during the oligotrophic summer period cyanobacteria biomass dominates the DCM after YD100 and diatoms start to contribute to the DCM after YD150, with a time lag of 50 days.

Lomas and Bates (2004) showed that the variability in the biomass of autotrophic eukaryotes was much higher than that of cyanobacteria and diatom taxonomic groups. Model results are consistent with this, and the model shows that the biomass of autotrophic eukaryotes increases up to four fold during the spring bloom period, whereas cyanobacteria and diatoms do not show any increase. The model suggests that top-down effects on algal group 1 are stronger compared to algal group 2, whereas growth of algal group 3 is bottom-up controlled (i.e. by phosphate limitation) during this period (Fig. 14f).

In the model there is a strong correlation between carbon production and export (not shown), although the export ratio is generally very low (Fig. 8c). This is in agreement with early studies on carbon flux in the ocean which hypothesized a direct link between particulate export production and primary production (e.g. Eppley and Peterson, 1979; Suess, 1980), with a predictable fraction of primary production being exported to the ocean interior. But observations at the oligotrophic time-series station BATS (Michaels et al., 1996; Steinberg et al., 2001), and other locations, show that the relationship between these two system parameters is highly variable when investigated on seasonally resolved time-scales. An early explanation for this variability was that some phytoplankton (e.g. large,

heavy diatoms) would contribute disproportionately to export production (e.g. Smetacek et al., 1984; Boyd and Newton, 1995, 1999). Although this size-based approach works for some systems, it does not seem to hold for the subtropical gyres where phytoplankton are small in size, have small sinking rates, and are tightly controlled by grazing. Steinberg et al. (2001) suggested that the observed weak correlation between carbon production and export can be due to physical events that affect the trapping efficiency and studies with new trap designs are needed to help address these issues.

Our model suggests that most of the export occurs during the spring bloom which is driven by the autotrophic eukaryotes (Fig. 3b) and thereby also dominates the mean export. Carbon production and flux to sinking material by diatoms remains very low during year 1998 (Fig. 10). Picoplankton have traditionally been viewed to contribute little to export production because of their small size and tight micrograzer control. However, there is sufficient evidence to dispute that notion. For example, Waite et al. (2000) found mass sedimentation of picoplankton embedded in aggregates. Pfannkuche and Lochte (1993) as well as Turley and Mackie (1995) found cyanobacteria in salp fecal pellets or aggregates, both by pigment analysis and by epifluorescene microscopy. Fecal pellets of copepods and tunicates in coastal Newfoundland waters were found to contain cyanobacteria in addition to nanoplankton (cells between 2 and 20 μm, including diatoms and coccolithophorids, Urban et al., 1993). Thus, there is still a need to at least offer a quantitative direct assessment of the role of pico- and nanoplankton groups in downward particle flux.

5.3. *Nutrient dynamics*

Knapp et al. (2005) hypothesized that even the relatively high nitrogen fixation rates would represent less than 10% of the new nitrogen supply to the BATS euphotic zone. Our model supports this hypothesis: switching off nitrogen fixation in the model results in a 9% decrease in new production (Table 4). This implies that it is unlikely that the nitrogen fixation is the missing nitrogen source for the DIC drawdown at BATS as previously suggested by Hansell and Carlson (2001), Hansell et al. (2004), and Knapp et al. (2005). Recently, Davis and McGillicudy (2006) used a video plankton recorder to estimate *Trichodesmium* abundance in the North Atlantic, and they hypothesized that deep colony abundance can be much higher than previously estimated and could potentially account for the missing nitrogen fixation. If further field studies prove this hypothesis is true, our model should be modified to include this deep nitrogen fixation process.

Simulations showed that nitrogen fixation and atmospheric deposition alone were not sufficient to support the observed primary production during the stratified oligotrophic period, although, when the higher nitrogen fixation estimates are used, surface nitrogen limitation on algal groups is reduced (not shown). Several previous studies (e.g. Moloney and Field, 1991; Anderson and Williams, 1998; Vallino, 2000) suggested that inclusion of DON cycling in ecosystem models can have important implications on the regulation of nutrient cycling. Our study builds on these studies and confirms that the model can only reproduce the observed primary production during the oligotrophic period when the DOM (i.e. DON and/or DOP) compartments are included. Although mesoscale nutrient inputs, whose magnitude is still debated (Oschlies and Garçon, 1998; Oschlies, 2002; McGillicuddy et al., 2003), are not considered in this model, model results agree well with low observed export ratio estimates (Fig. 8c) that suggest that most of the production during this period is regenerated production. When the DOM compartment is not included and particulate organic matter (i.e. detritus in the model) is directly remineralized into nutrients, primary production fades away after the spring bloom as detritus compartments sink out of the surface waters. Because DOM does not sink and instead gradually transforms into nutrients, it can support the production in the surface waters during the oligotrophic period. Recent data (Burke et al., 2007) show that particulate phosphorus export is very high during the oligotrophic period and inorganic phosphate cannot support this export term. However, there is a decrease in the integrated euphotic zone DOP pool that matches the phosphorus export (Burke et al., 2007). This observation helps to mechanistically link the carbon and phosphorus cycles in the Sargasso Sea, but also supports the hypothesis that the Sargasso Sea is phosphate limited.

Recent literature suggests that phytoplankton cellular nutrient stoichiometry may show strong deviations from the Redfield ratio (cf. Section 2.1, Table 2). Our model results show that cellular

nutrient stoichiometry of phytoplankton can play an important role in controlling the ambient nutrient stoichiometry in the surface waters of the Sargasso Sea. Using the Redfield stoichiometry for cellular nutrient uptake and growth may result in a high decrease in algal carbon production (Table 4) during the oligotrophic summer period (Fig. 11a). Thus, deviations from the Redfield ratio for uptake of nutrients emerge as an important factor that controls carbon production in the region. When the simulated algal groups follow the Redfield stoichiometry for uptake, less nitrogen is removed from the surface waters (Figs. 12a and b) and less carbon can be fixed by algal groups (35% less, Table 4) resulting in a smaller DIC drawdown.

Wu et al. (2000) argued that phosphate depletion in Sargasso Sea surface waters can be attributed to the high nitrate to phosphate ratio (20–32) in the upper nutricline relative to planktonic 16 N:1 P ratio. Our model results also find that during the spring bloom period in the surface waters, nanomolar nitrate to nanomolar phosphate ratios can be higher than the Redfield ratio. On the other hand, average phytoplanktonic N:P uptake can also exceed the Redfield ratio. Thus, it is the balance between the amount of excess ambient nitrogen and the amount of excess nitrogen that the phytoplankton can take up which determines the ambient N:P ratio. For example, the model suggests that surface (0–50 m) nitrate to phosphate ratios may be lower than the Redfield ratio during the oligotrophic summer period (Fig. 13a). During this period phytoplankton nutrient uptake can follow an N:P ratio higher than the Redfield ratio and because of low ambient nutrient levels phytoplankton can pull the ambient nitrogen to phosphorus ratios to below Redfield values. Therefore observations which are taken during spring (i.e. Wu et al., 2000) in the Sargasso Sea may not necessarily represent the underlying mechanism of the nutrient stoichiometry in the region during the whole year. Phosphate depletion during the spring period can be due to high ambient nitrate to phosphate ratios, whereas community structure may shift the system to a lower ambient nitrate to phosphate ratio during the oligotrophic period. Sensitivity tests with cellular nutrient ratios fixed close to the Redfield ratio show that if the phytoplanktonic ratio was 16 N:1 P then the hypothesis developed by Wu et al. (2000) can be valid for the whole year. The ambient phosphate would be depleted before nitrate (Figs. 12a and c) and the ambient nitrate to phosphate ratios would be higher than the Redfield ratio (Figs. 13c and d).

Wu et al. (2000) also raise the question why there should be nitrogen fixation near Bermuda if nitrate to phosphate ratios are higher than the Redfield ratio. The model results indicate that under nutrient deplete conditions at BATS the cellular nutrient requirements by small phytoplankton can be higher than the Redfield N:P ratios. Also, high nitrate to phosphate ratios do not necessarily mean that nitrate cannot be limiting. Our model results suggest that surface nitrate values can be lower ($<0.1\,\mu mol\,l^{-1}$) than required by phytoplankton groups (Figs. 14a–c) and presumably by nitrogen fixers as well. It is known that nitrogen fixers are not very efficient in inorganic nutrient uptake (McCarthy and Carpenter, 1979; Mulholland and Capone, 1999).

Non-Redfield nutrient uptake by algal groups also has implications on uncoupling between the modeled export and f-ratios (Fig. 8c). Lipschultz (2001) documented that the annual averaged f-ratios estimated by using the nitrate and ammonium assimilation rates were 0.39 and 0.08, whereas observed export ratios were 0.019 and 0.023 for years 1992 and 1993 (Hood et al., 2001), respectively. Modeled f-ratios for year 1998 were also higher than the export ratios (0.11 vs 0.079), whereas the results of the sensitivity test done by setting the cellular nutrient ratios close to the Redfield ratio show that the f-ratios are considerably lower (annual average of 0.04) than the export ratios (annual average of 0.1). Model results suggest that there can be uncoupling between nitrate uptake and primary production under phosphate limiting conditions. Algal groups continue to take up nitrate (Figs. 14a–c) while their growth is limited by phosphate (Figs. 14d–f), resulting in a higher f-ratio. If the nutrient uptake by algal groups is assumed to be constant and they are not allowed to take up excess nitrate, then the f-ratios may be reduced considerably by low nitrate uptake under phosphorus-limited conditions.

5.4. Role of phosphorus

The model results are in agreement with limited observational evidence for phosphorus limitation in the Sargasso Sea (Scanlan and Wilson, 1999; Lomas et al., 2004). In the model, phosphorus limitation is found even for small cyanobacteria species (Fig. 14d) which is in agreement with observations

(Scanlan and Wilson, 1999; Moore et al., 2005). It was observed that in the Sargasso Sea during the stratified summer period ~30% of the autotrophic eukaryotes in the surface waters were phosphorus limited and in the well-mixed fall period 70% were limited by phosphorus availability (Lomas et al., 2004). Simulation results support the hypothesis by Lomas et al. (2004) that phosphorus stress on phytoplankton differs among algal groups and different seasons in the Sargasso Sea. Simulation results suggest that all algal groups are phosphorus limited in the surface waters; however, this limitation is stronger on microphytoplankton and autotrophic eukaryotes relative to cyanobacteria (Figs. 14d–f), which also agrees well with the observations (i.e. Lomas et al., 2004). Implicitly including nitrogen fixation into the model dynamics resulted in neglecting the possible phosphate uptake by nitrogen fixers (Wu et al., 2000). However, considering the low *Trichodesmium* abundance in the region (Orcutt et al., 2001), and possible phosphorus limitation (Wu et al., 2000) on these species, this may not have a strong influence on the modeled phosphorus distribution. This would also not affect our conclusion on phosphorus limitation, because uptake by diazotrophs would only increase the existing phosphorus limitation.

The study by Mongin et al. (2003) suggests that there is no nutrient limitation on phytoplankton groups during the winter and spring period. Although our results are in agreement with that study that algal groups are limited by nitrogen (nitrate + ammonium) through the upper 60 m during the year other than winter and spring periods (Figs. 14a–c), our results further show that algal groups can be limited by phosphorus even during the winter and spring periods (Figs. 14d–f).

Results of the cell quota algal group model suggest that silicate may play a relatively minor role limiting diatoms. This is in agreement with Mongin et al. (2003) but contradicts with Brzezinski and Nelson (1996) and Lima and Doney (2004), which suggested silicate limitation of diatom growth rates.

6. Conclusions

Our model results show that the ability of algal groups to regulate their nutrient uptake mechanism and the DON and DOP dynamics are the two main factors that sustain the observed primary production during the oligotrophic summer period. Nitrogen fixation and atmospheric nitrogen deposition are secondary factors fueling production during this period. Therefore, regulation of phytoplankton elemental ratios by environmental conditions can be an important component of the ocean carbon export which should be considered in carbon cycle models.

Previous modeling studies performed for this region have widely ignored the role of phosphorus on algal growth, because nitrogen is considered to be the most important nutrient that limits algal growth. Our study builds on recent observations that appreciate the potential importance of phosphorus as a limiting nutrient. Results of this study suggest that the phosphorus limitation can be more important than previously thought and phosphate limits the growth of all algal groups throughout the year, whereas moderate nitrogen limitation takes place during the oligotrophic summer period. Phosphate can be limiting even during the bloom period, although nitrogen does not limit algal growth during this period. Phosphate limitation is especially strong for larger diatom and autotrophic eukaryotes groups, although smaller cyanobacteria forms also experience phosphate limitation throughout the year. In order to understand the controlling mechanisms of primary production today, and in the future as the oceans respond to climate change, we need to consider phosphorus together with nitrogen, silicon, and iron.

It has been previously shown (Fasham et al., 1990; Spitz et al., 2001; Anderson and Pondaven, 2003) that the inclusion of DON utilization and breakdown would improve the fit of models to BATS data. To our knowledge our model was the first to show the importance of including both DON and DOP dynamics. In our model, heterotrophic bacteria was not explicitly included but their effect was treated as a remineralization process. Uptake kinetics of DON and DOP by bacteria may be integral in correctly representing the DON and DOP cycles and a bacterial component together with carbon, nitrogen, and phosphorus stoichiometry of both bacterial and algal growth may have to be included in carbon cycle models as more observations become available. Another process that is neglected in the current modeling study is the variability of zooplankton elemental ratios. If grazer C:N:P ratios differ significantly from those of their prey, the regenerated nutrient flux may change the nutrient dynamics (Sterner and Elser, 2002) and, potentially, the limiting nutrients. Influence of

horizontal physical processes on the biogeochemical dynamics is not included in this study, but efforts to include a simplified version of the ecosystem model used in this study in a North Atlantic circulation model are underway.

Acknowledgments

Supported by EU contract no SIP3-CT-2003-502885 to LEGOS/CNRS, part of WP7 from IP-MERSEA project. M.W.L. acknowledges support of the NSF Chemical and Biological Oceanography programs through awards OCE-0326885 and OCE-0453023. This is BIOS Contribution no. 1699. We thank K.E. Taylor for providing the skill assessment tools. We acknowledge Isabelle Dadou for providing useful discussions and details of the Taylor diagram. We also thank two anonymous reviewers for constructive comments on an earlier version of the manuscript.

References

Ammerman, J.W., Hood, R.R., Case, D.A., Cotner, J.B., 2003. Phosphorus deficiency in the Atlantic: an emerging paradigm in oceanography. EOS Transactions-American Geophysical Union 84, 165–170.

Anderson, R., Bidigare, R., Keller, M., Latasa, M., 1996. A comparison of HPLC pigment signatures and electron microscopic observations for oligotrophic waters of the North Atlantic and Pacific Oceans. Deep-Sea Research II 43, 517–537.

Anderson, T., Pondaven, P., 2003. Non-Redfield carbon and nitrogen cycling in the Sargasso Sea: pelagic imbalances and export flux. Deep-Sea Research I 50 (5), 573–591.

Anderson, T.R., Williams, P.J.l., 1998. Modelling the seasonal cycle of dissolved organic matter at Station E1 in the English Channel. Estuarine, Coastal and Shelf Science 46, 93–109.

Andersson, A., Lee, C., Azam, F., Hagstrom, A., 1985. Release of amino acids and inorganic nutrients by heterotrophic marine microflagellates. Marine Ecology Progress Series 23, 99–106.

Azam, F., Hodson, R.E., 1977. Size distribution and activity of marine microheterotrophs. Limnology and Oceanography 22, 492–501.

Baker, A.R., Kelly, S.D., Biswas, K.F., Witt, M., Jickells, T.D., 2003. Atmospheric deposition of nutrients to the Atlantic Ocean. Geophysical Research Letters 30.

Bates, N.R., Hansell, D.A., 2004. Temporal variability of excess nitrate in the Subtropical Mode Water of the North Atlantic Ocean. Marine Chemistry 84, 225–241.

Benitez-Nelson, C., 2000. The biogeochemical cycling of phosphorus in marine systems. Earth-Science Review 51, 109–135.

Bertilsson, S., Berglund, O., Karl, D.M., Chisholm, S.W., 2003. Elemental composition of marine *Prochlorococcus* and *Synechococcus*: implications for the ecological stoichiometry of the sea. Limnology and Oceanography 48, 1721–1731.

Bidigare, R.R., 1983. Nitrogen excretion in Marine zooplankton. In: Carpenter, E.J., Capone, D.G. (Eds.), Nitrogen in the Marine Environment. Academic Press, New York, pp. 385–409.

Bissett, W.P., Walsh, J.J., Dieterle, D.A., Carder, K.L., 1999a. Carbon cycling in the upper waters of the Sargasso Sea: 1. Numerical simulation of differential carbon and nitrogen fluxes. Deep-Sea Research I 46 (2), 205–269.

Bissett, W.P., Walsh, J.J., Dieterle, D.A., Carder, K.L., 1999b. Carbon cycling in the upper waters of the Sargasso Sea: II. Numerical simulation of apparent and inherent optical properties. Deep-Sea Research I 46 (2), 271–317.

Boyd, P., Newton, P., 1995. Evidence of the potential influence of planktonic community structure on the interannual variability of particulate organic-carbon flux. Deep-Sea Research I 42, 619–639.

Boyd, P., Newton, P., 1999. Does planktonic community structure determine downward particulate organic carbon flux in different oceanic provinces? Deep-Sea Research I 46, 63–91.

Bronk, D.A., 2002. Dynamics of DON. In: Hansell, D.A., Carlson, C.A. (Eds.), Biogeochemistry of Marine Dissolved Organic Matter. Academic Press, New York, pp. 153–250.

Brzezinski, M., Nelson, D., 1996. Chronic substrate limitation of silicic acid uptake rates in the western Sargasso Sea. Deep-Sea Research II 43, 437–453.

Burke, A.L., Lomas, M.W., Ammerman, J.W., Dyhrman, S.D., 2007. Does assimilation of dissolved organic phosphorus support particulate phosphorus export flues in the Sargasso Sea? Abstracts at Aquatic Sciences Meeting, Santa Fe 2007.

Campbell, L., Vaulot, D., 1993. Photosynthetic picoplankton community structure in the Subtropical North Pacific Ocean near Hawaii (station ALOHA). Deep-Sea Research I 40, 2043–2060.

Capone, D.G., Zehr, J., Paerl, H., Bergman, B., Carpenter, E.J., 1997. A globally significant marine cyanobacterium. Science 276, 1221–1229.

Capone, D.G., Burns, J.A., Montoya, J.P., Subramaniam, A., Mahaffey, C., Gunderson, T., Michaels, A.F., 2005. Nitrogen fixation by *Trichodesmium* spp.: an important source of new nitrogen to the tropical and subtropical North Atlantic Ocean. Global Biogeochemical Cycles 19.

Carlson, C., Ducklow, H.W., 1996. Growth of bacterioplankton and consumption of dissolved organic carbon in the Sargasso Sea. Aquatic Microbial Ecology 10, 68–85.

Carlson, C.A., 2002. Production and removal processes. In: Hansell, D.A., Carlson, C.A. (Eds.), Biogeochemistry of Marine Dissolved Organic Matter. Academic Press, New York, pp. 91–151.

Carpenter, E.J., Montoya, J.P., Burns, J., Mulholland, M., Subramaniam, A., Capone, D.G., 1999. Extensive bloom of a N_2 fixing symbiotic association in the tropical Atlantic Ocean. Marine Ecology Progress Series 185, 273–283.

Casey, J.R., Lomas, M.W., Mandecki, J., Walker, D.E., 2007. *Prochlorococcus* contributes to new production in the Sargasso Sea deep chlorophyll maximum. Geophysical Research Letters 34.

Cavender-Bares, K.K., Karl, D.M., Chisholm, S.W., 2001. Nutrient gradients in the western North Atlantic Ocean: relationship to microbial community structure and comparison to patterns in the Pacific Ocean. Deep-Sea Research I 48, 2373–2395.

Charria, G., Dadou, I., Drevillon, M., Llido, J., Garçon, V., February 2006. Coupled physical/biogeochemical modelling at mesoscale in the North Atlantic Ocean: Rossby waves, an example of coupled process. MERCATOR Ocean Quaterly Newsletter.

Christian, J.R., Karl, D.M., 1995. Bacterial ectoenzymes in marine waters: activity ratios and temperature responses in three oceanic provinces. Limnology and Oceanography 40, 1042–1049.

Christian, J.R., Verschell, M.A., Murtugudde, R., Busalacchi, A.J., McClain, C.R., 2002. Biogeochemical modelling of the tropical Pacific Ocean. I. Seasonal and interannual variability. Deep-Sea Research II 49, 509–543.

Crank, J., 1956. The Mathematics of Diffusion. Oxford University Press, Oxford.

Cuhel, R.L., Waterbury, J.B., 1984. Biochemical composition and short term nutrient incorporation patterns in a unicellular marine cyanobacterium, *Synechococcus* (WH7803). Limnology and Oceanography 29 (2), 370–374.

Dadou, I., Evans, G., Garçon, V., 2004. Using JGOFS *in situ* and ocean color data to compare biogeochemical models and estimate their parameters in the subtropical North Atlantic Ocean. Journal of Marine Research 62 (4), 565–594.

Dam, H.G., Zhang, X., Butler, M., Roman, M.R., 1995. Mesozooplankton grazing and metabolism at the equator in the central Pacific: implications for carbon and nitrogen fluxes. Deep-Sea Research II 42 (2–3), 735–756.

Davis, C.S., McGillicudy, D.J., 2006. Transatlantic abundance of the N_2-fixing colonial cyanobacterium *Trichodesmium*. Science 312, 1517–1520.

Doney, S.C., Glover, D.M., Najjar, R.G., 1996. A new coupled, one-dimensional biological–physical model for the upper ocean: applications to the JGOFS Bermuda Atlantic Time-series Study (BATS) site. Deep-Sea Research II 43, 591–624.

Dore, J.E., Karl, D.M., 1996. Nitrification in the euphotic zone as a source for nitrite, nitrate, and nitrous oxide at Station ALOHA. Limnology and Oceanography 41, 1619–1628.

Droop, M.R., 1973. Some thoughts on nutrient limitation in algae. Journal of Phycology 9 (3), 264–272.

Dunne, J.P., Murray, J.W., 1999. Sensitivity of ^{234}Th export to physical processes in the Central Equatorial Pacific. Deep-Sea Research I 46, 831–854.

DuRand, M.D., Olson, R.J., Chisholm, S.W., 2001. Phytoplankton population dynamics at the Bermuda Atlantic time series station in the Sargasso Sea. Deep-Sea Research II 48 (8–9), 1983–2003.

Eppley, R.W., 1972. Temperature and phytoplankton growth in the sea. Fishery Bulletin 70, 1063–1085.

Eppley, R.W., Peterson, B.J., 1979. Particulate organic matter flux and planktonic organic matter in the surface layer of the ocean. Deep-Sea Research 30, 311–323.

Fanning, K.A., 1992. Nutrient provinces in the sea: concentration ratios, reaction rate ratios, and ideal co-variation. Journal of Geophysical Research 97, 5693–5712.

Fasham, M., Ducklow, H.W., McKelvie, D.S., 1990. A nitrogen-based model of plankton dynamics in the oceanic mixed layer. Journal of Marine Research 48, 591–639.

Ferrier-Pages, C., Karner, M., Rassoulzadegan, F., 1998. Release of dissolved amino acids by flagellates and ciliates grazing on bacteria. Oceanologica Acta 21, 485–494.

Flynn, K.J., Davidson, K., Leftley, J.W., 1994. Carbon–nitrogen relations at whole-cell and free-amino-acid levels during batch growth of *Isochrysis galbana* (prymnesiophyceae) under conditions of alternating light and dark. Marine Biology 118 (2), 229–237.

Franks, P.J.S., Wroblewski, J.S., Flierl, G.R., 1986. Behavior of a simple plankton model with food-level acclimation by herbivores. Marine Biology 91 (1), 121–129.

Geider, R.J., La Roche, J., 2002. Redfield revisited: variability in the N:P ratio of phytoplankton and its biochemical basis. European Journal of Phycology 37, 1–17.

Geider, R.J., MacIntyre, H.L., Kana, T.M., 1998. A dynamic regulatory model of phytoplanktonic acclimation to light, nutrients, and temperature. Limnology and Oceanography 43 (4), 679–694.

Gin, K.Y.H., Chisholm, S.W., Olson, R.J., 1999. Seasonal and depth variation in microbial size spectra at the Bermuda Atlantic Time Series station. Deep-Sea Research I 46, 1221–1245.

Gregg, W.W., Carder, K.L., 1990. A simple spectral solar irradiance model for cloudless maritime atmospheres. Limnology and Oceanography 35 (8), 1657–1675.

Gruber, N., Sarmiento, J.J., 1997. Global patterns of marine nitrogen fixation and denitrification. Global Biogeochemical Cycles 11 (2), 235–266.

Gruber, N., Sarmiento, J.L., 2002. Large-scale biogeochemical–-physical interactions in elemental cycles. In: Robinson, A.R., McCarthy, J.J., Rothschild, B.J. (Eds.), The Sea, vol. 12. Wiley, New York, pp. 337–399.

Haney, J.A., Jackson, G.A., 1996. Modeling phytoplankton growth rates. Journal of Plankton Research 18 (1), 63–85.

Hansell, D.A., Carlson, C.A., 2001. Biogeochemistry of total organic carbon and nitrogen in the Sargasso Sea: control by convective overturn. Deep-Sea Research II 48, 1649–1667.

Hansell, D.A., Bates, N.R., Olson, D.B., 2004. Excess nitrate and nitrogen fixation in the North Atlantic Ocean. Marine Chemistry 84, 243–265.

Harrison, W.G., Harris, L.R., Irwin, B.D., 1996. The kinetics of nitrogen utilization in the oceanic mixed layer: nitrate and ammonium interactions at nanomolar concentrations. Limnology and Oceanography 41 (1), 16–32.

Hastings, M.G., Sigman, D.M., Lipschultz, F., 2003. Isotopic evidence for source changes of nitrate in rain at Bermuda. Journal of Geophysical Research 108 (D24).

Hebel, D.V., Karl, D.M., 2001. Seasonal, interannual and decadal variations in particulate matter concentrations and composition in the subtropical North Pacific Ocean. Deep-Sea Research II 48 (8), 1669–1695.

Hedges, J.I., 2002. Why dissolved organics matter. In: Hansell, D.A., Carlson, C.A. (Eds.), Biogeochemistry of Marine Dissolved Organic Matter. Academic Press, New York, pp. 1–33.

Ho, T.-Y., Quigg, A., Finkel, Z.V., Milligan, A.J., Wyman, K., Falkowski, P.G., Morel, F.M.M., 2003. Elemental composition of some eukaryotic marine phytoplankton. Journal of Phycology 39, 1145–1159.

Hood, R.R., Bates, N.R., Capone, D.G., Olson, D.B., 2001. Modeling the effects of nitrogen fixation on carbon and nitrogen fluxes at BATS. Deep-Sea Research II 48 (8–9), 1609–1648.

Hurrell, J.W., Kushnir, Y., Ottersen, G., Visbeck, M., 2003. An overview of the North Atlantic Oscillation. In: Hurrell, J.W., Kushnir, Y., Ottersen, G., Visbeck, M. (Eds.), The North

Atlantic Oscillation: Climate Significance and Environmental Impact. American Geophysical Union, pp. 1–36.

Hutchins, D.A., Bruland, K.W., 1995. Fe, Zn, Mn and N transfer between size classes in a coastal phytoplankton community: trace metal and major nutrient recycling compared. Journal of Marine Research 53 (2), 297–313.

Ivlev, V.S., 1955. Experimental Ecology of the Feeding of Fishes. Yale University Press, New Haven (translated from Russian by D. Scott).

Jackson, G.A., Burd, A.B., 1998. Aggregation in the marine environment: a critical review. Environmental Science and Technology 32, 2805–2814.

Jenkins, W.J., 1988. Nitrate flux into the euphotic zone near Bermuda. Nature 331, 521–523.

Jumars, P.A., Penry, D.L., Baross, J.A., Perry, M.J., Frost, B.W., 1989. Closing the microbial loop: dissolved carbon pathway to heterotrophic bacteria from incomplete ingestion, digestion and absorption in animals. Deep-Sea Research 36, 483–495.

Kallberg, P., Simmons, A., Uppala, S., Fuentes, M., 2004. The ERA-40 archive. Technical Report 17, ECMWF, Shinfield Park, Reading.

Kana, T.M., Glibert, P.M., 1987. Effect of irradiances up to $2000\,\mu E\,m^{-2}\,s^{-1}$ on marine *Synechococcus* WH7803. I. Growth, pigmentation, and cell composition. Deep-Sea Research 34 (4A), 479–495.

Karl, D.M., Bjorkman, K.M., 2002. Dynamics of DOP. In: Hansell, D.A., Carlson, C.A. (Eds.), Biogeochemistry of Marine Dissolved Organic Matter. Academic Press, New York, pp. 250–367.

Knapp, A.N., Sigman, D.M., Lipschultz, F., 2005. N isotopic composition of dissolved organic nitrogen and nitrate at the Bermuda Atlantic Time-series Study site. Global Biogeochemical Cycles 19 (1).

Lampitt, R.S., 1990. What happens to zooplankton fecal pellets? Implications for material flux. Marine Biology 104, 15–23.

Landry, M.R., Kirshtein, J., Constantinou, J., 1995. A refined dilution technique for measuring the community grazing impact of microzooplankton, with experimental tests in the central equatorial Pacific. Marine Ecology Progress Series 120 (1–3), 53–63.

Landry, M.R., Kirshtein, J., Constantinou, J., 1996. Abundances and distributions of picoplankton populations in the central equatorial Pacific from 12°N to 12°S, 140°W. Deep-Sea Research II 43 (4–6), 871–890.

Laws, E.A., Bannister, T.T., 1980. Nutrient- and light-limited growth of *Thalassiosira fluviatilis* in continious culture, with implications for phytoplankton growth in the ocean. Limnology and Oceanography 25 (3), 457–473.

Laws, E.A., Falkowski, P.G., Smith, W.O., Ducklow, H., McCarthy, J.J., 2000. Temperature effects on export production in the open ocean. Global Biogeochemical Cycles 14, 1231–1246.

Ledwell, J.R., Watson, A.J., Law, C.S., 1998. Mixing of a tracer in the pycnocline. Journal of Geophysical Research 103 (C10), 21499–21529.

Lee, K., Karl, D.M., Wanninkhof, R., Zhang, J., 2002. Global estimates of net carbon production in the nitrate-depleted tropical and subtropical oceans. Geophysical Research Letters 29 (1907).

Leonard, C.L., McClain, C.R., Murtugudde, R., Hofmann, E.E., Harding, L.W.J., 1999. An iron-based ecosystem model of the central equatorial Pacific. Journal of Geophysical Research 104 (C1), 1325–1341.

Leonardos, N., Geider, R.J., 2004. Effects of nitrate: phosphate supply ratio and irradiance on the C:N:P stoichiometry of *Chaetocerosmuelleri*. European Journal of Phycology 39, 173–180.

Li, W.K.W., Zohary, T., Yacobi, Y.Z., Wood, A.M., 1993. Ultraphytoplankton in the eastern Mediterranean Sea: towards deriving phytoplankton biomass from flow cytometric measurements of abundance fluorescence and light scatter. Marine Ecology Progress Series 102, 79–87.

Lima, I.D., Doney, S.C., 2004. A three-dimensional, multinutrient, and size-structured ecosystem model for the North Atlantic. Global Biogeochemical Cycles 18.

Lipschultz, F., 2001. A time series assessment of the nitrogen cycle in the Sargasso Sea. Deep-Sea Research II 48 (8–9), 1897–1924.

Lipschultz, F., Bates, N., Carlson, C., Hansell, D., 2002. New production in the Sargasso Sea: history and current status. Global Biogeochemical Cycles 16, 1–16.

Lomas, M.W., Bates, N.R., 2004. Potential controls on interannual partitioning of organic carbon during the winter/spring phytoplankton bloom at the Bermuda Atlantic Time-series Study (BATS) site. Deep-Sea Research I 51, 1619–1636.

Lomas, M.W., Swain, A., Shelton, R., Ammerman, J.A., 2004. Taxonomic variability of phosphorus stress in Sargasso Sea phytoplankton. Limnology and Oceanography 49, 2303–2310.

Madin, L.P., Horgan, E.F., Steinberg, D.K., 2001. Zooplankton at the Bermuda Atlantic Time-series Study (BATS) station: diel, seasonal and interannual variation in biomass. Deep-Sea Research II 48 (8–9), 2063–2082.

Mahaffey, C., Williams, R.G., Wolff, G.A., Anderson, W.T., 2004. Physical supply of nitrogen to phytoplankton in the Atlantic Ocean. Global Biogeochemical Cycles 18.

Marra, J., Bidigare, R.R., Dickey, T.D., 1990. Nutrients and mixing, chlorophyll and phytoplankton growth. Deep-Sea Research 37 (1A), 127–143.

McCarthy, J.J., Carpenter, E.J., 1979. Oscillatoria (*Trichodesmium*) *thiebautii* (*Cyanophyta*) in the central North Atlantic Ocean. Journal of Phycology 15, 75–82.

McGillicuddy, D.J., Anderson, L.A., Doney, S.C., Maltrud, M.E., 2003. Eddy-driven sources and sinks of nutrients in the upper ocean: results from a 0.1 degree resolution model of the North Atlantic. Global Biogeochemical Cycles 17 (2).

McGillicuddy, D.J., Anderson, L.A., Bates, N.R., Bibby, T., Buesseler, K.O., Carlson, C.A., Davis, C.S., Ewart, C., Falkowski, P.G., Goldthwait, S.A., Hansell, D.A., Jenkins, W.J., Johnson, R., Kosnyrev, V.K., Ledwell, J.R., Li, Q.P., Siegel, D.A., Steinberg, D.K., 2007. Eddy/wind interactions stimulate extraordinary mid-ocean plankton blooms. Science 316.

Menzel, D.W., Ryther, J.H., 1961. Annual variations in primary production of the Sargasso Sea off Bermuda. Deep-Sea Research 7, 282–288.

Michaels, A.F., Knap, A.H., Dow, R.L., Gundersen, K., Johnson, R.J., Sorensen, J., Close, A., Knauer, G.A., Lohrenz, S.E., Asper, V.A., Tuel, M., Bidigare, R.R., 1994. Seasonal patterns of biogeochemistry at the US JGOFS Bermuda Atlantic Time-series Study side. Deep-Sea Research I 41, 1013–1038.

Michaels, A.F., Olson, D., Sarmiento, J., Ammerman, J., Fanning, K., Jahnke, R., Knap, A., Lipschultz, F., Prospero, J., 1996. Inputs, losses and transformations of nitrogen and phosphorus in the deep North Atlantic Ocean. Biogeochemistry 35, 181–226.

Moloney, C.L., Field, J.G., 1991. The size-based dynamics of plankton food webs. Journal of Plankton Research 13, 1003–1038.

Mongin, M., Nelson, D.M., Pondaven, P., Brzezinski, M.A., Treguer, P., 2003. Simulation of upper-ocean biogeochemistry with a flexible-composition phytoplankton model: C, N and Si cycling in the western Sargasso Sea. Deep-Sea Research I 50, 1445–1480.

Montoya, J., Holl, C., Zehr, J., Hansen, A., Villareal, T.A., Capone, D.G., 2004. High rates of N_2 fixation by unicellular diazotrophs in the oligotrophic Pacific Ocean. Nature 430, 1027–1032.

Moore, L.R., Goericke, R., Chisholm, S.W., 1995. Comparative physiology of *Synechococcus* and *Prochlorococcus*: influence of light and temperature on growth, pigments, fluorescence and absorptive properties. Marine Ecology Progress Series 116 (1–3), 259–275.

Moore, L.R., Post, A.F., Rocap, G., Chisholm, S.W., 2002. Utilization of different nitrogen sources by the marine cyanobacteria *Prochlorococcus* and *Synechococcus*. Limnology and Oceanography 47 (4), 989–996.

Moore, L.R., Ostrowski, M., Scanlan, D.J., Feren, K., Sweetsir, T., 2005. Ecotypic variation in phosphorus-acquisition mechanisms within marine picocyanobacteria. Aquatic Microbial Ecology 39, 257–269.

Mulholland, M.R., Capone, D.G., 1999. Nitrogen fixation, uptake and metabolism in natural and cultured populations of *Trichodesmium* spp. Marine Ecology Progress Series 188, 33–49.

Nagata, T., 2000. Production mechanisms of dissolved organic matter. In: Kirchman, D. (Ed.), Microbial Ecology of the Oceans. Wiley, New York, pp. 121–152.

Nagata, T., Kirchman, D.L., 1991. Release of dissolved free and combined amino acids by bacterivorous marine flagellates. Limnology and Oceanography 36, 433–443.

Nelson, D., Brzezinski, M., 1997. Diatom growth and productivity in an oligotrophic midocean gyre: a 3-yr record from the Sargasso Sea near Bermuda. Limnology and Oceanography 43, 473–486.

Nelson, D.M., Treguer, P., 1992. Role of silicon as a limiting nutrient to antarctic diatoms: evidence from kinetic studies in the Ross Sea ice-edge zone. Marine Ecology Progress Series 80, 255–264.

Nelson, D.M., Treguer, P., Brzezinski, M.A., Leynaert, A., Queaguiner, B., 1995. Production and dissolution of biogenic silica in the ocean: revised global estimates, comparison with regional data and relationship to biogenic sedimentation. Global Biogeochemical Cycles 9, 359–372.

Orcutt, K.M., Lipschultz, F., Gundersen, K., Arimoto, R., Michaels, A.F., Knap, A.H., Gallon, J.R., 2001. A seasonal study of the significance of N_2 fixation by *Trichodesmium* spp. at the Bermuda Atlantic Time-series Study (BATS) site. Deep-Sea Research II 48 (8–9), 1583–1608.

Oschlies, A., 2001. NAO-induced long-term changes in nutrient supply to the surface waters of the North Atlantic. Geophysical Research Letters 28, 1751–1754.

Oschlies, A., 2002. Can eddies make ocean deserts bloom? Global Biogeochemical Cycles 16.

Oschlies, A., Garçon, V., 1998. Eddy-induced enhancement of primary production in a model of the North Atlantic Ocean. Nature 394, 266–269.

Parpais, J., Marie, D., Partensky, F., Morin, P., Vaulot, D., 1996. Effect of phosphorus starvation on the cell cycle of the photosynthetic prokaryote prochlorococcus. Marine Ecology Progress Series 132, 265–274.

Partensky, F., Hoepffner, N., Li, W.K.W., Ulloa, O., Vaulot, D., 1993. Photoacclimation of *Prochlorococcus* sp. (Prochlorophyta) strains isolated from the North Atlantic and the Mediterranean Sea. Plant Physiology 101 (1), 285–296.

Pfannkuche, O., Lochte, K., 1993. Open ocean pelago-benthic coupling—cyanobacteria as tracers of sedimenting salp feces. Deep-Sea Research I 40, 727–737.

Pomeroy, L.R., 1974. The oceans's food web, a changing paradigm. Bioscience 24, 499–504.

Redfield, A.C., Ketchum, B.H., Richards, F.A., 1963. The influence of organisms on the composition of seawater. In: Hill, M.N. (Ed.), The Sea. The Composition of Seawater, vol. 2. Wiley, New York, pp. 26–77.

Roman, M.R., Gauzens, A.L., 1997. Copepod grazing in the equatorial Pacific. Limnology and Oceanography 42 (4), 623–634.

Roman, M.R., Adolf, H.A., Landry, M.R., Madin, L.P., Steinberg, D.K., Zhang, X., 2002. Estimates of oceanic mesozooplankton production: a comparison using the Bermuda and Hawaii time-series data. Deep-Sea Research II 49, 175–192.

Ryther, J.H., Menzel, D.W., 1960. The seasonal and geographical range of primary production in the western Sargasso Sea. Deep-Sea Research 6, 235–238.

Sakshaug, E., Andresen, K., Kiefer, D.A., 1989. A steady state description of growth and light absorption in the marine planktonic diatom *Skeletonema costatum*. Limnology and Oceanography 34 (1), 198–205.

Salihoglu, B., 2005. Modeling the effects of physical and biogeochemical processes on phytoplankton species and carbon production in the equatorial Pacific Ocean. Ph.D. Thesis, Old Dominion University.

Salihoglu, B., Hofmann, E.E., 2007. Simulations of phytoplankton species and carbon production in the equatorial Pacific Ocean 1. Model configuration and ecosystem dynamics. Journal of Marine Research 65, 219–273.

Scanlan, D.J., Wilson, W.H., 1999. Application of molecular techniques to addressing the role of P as a effector in marine ecosystems. Hydrobiologia 401, 149–175.

Schartau, M., Oschlies, A., 2003a. Simultaneous data based optimization of a 1D-ecosystem model at three locations in the North Atlantic: part II—method and parameter estimates. Journal of Marine Research 61, 765–793.

Schartau, M., Oschlies, A., 2003b. Simultaneous data based optimization of a 1D-ecosystem model at three locations in the North Atlantic: part II—standing stocks and nitrogen fluxes. Journal of Marine Research 61, 795–821.

Siegel, D.A., McGillicuddy, D.J., Fields, E.A., 1999. Mesoscale eddies, satellite altimetry, and new production in the Sargasso Sea. Journal of Geophysical Research 104, 13359–13379.

Smetacek, V., von Bodungen, B., Knoppers, B., Peinert, R., Pollehne, F., Stegman, P., Zeitzschel, B., 1984. Seasonal stages characterizing the annual cycle of an inshore pelagic system. International Council for the Exploration of the Sea 183, 126–135.

Spitz, Y.H., Moisan, J.R., Abbott, M.R., 2001. Configuring an ecosystem model using data from the Bermuda-Atlantic Time Series (BATS). Deep-Sea Research II 48 (8–9), 1733–1768.

Spokes, L.J., Yeatman, S., Cornell, S., Jickells, T., 2000. Nitrogen deposition to the eastern Atlantic Ocean. The importance of south-easterly flow. Tellus 52B, 37–49.

Steinberg, D.K., Carlson, C.A., Bates, N.R., Goldthwait, S.A., Madin, L.P., Michaels, A.F., 2000. Zooplankton vertical migration and the active transport of dissolved organic and inorganic carbon in the Sargasso Sea. Deep-Sea Research I 47, 137–158.

Steinberg, D.K., Carlson, C.A., Bates, N.R., Johnson, R.J., Michaels, A.F., Knap, A., 2001. Overview of the US JGOFS Bermuda Atlantic Time-series Study (BATS): a decade-scale look at ocean biology and biogeochemistry. Deep-Sea Research II 48, 1405–1448.

Steinberg, D.K., Goldthwait, S.A., Hansell, D., 2002. Zooplankton vertical migration and the active transport of dissolved organic and inorganic nitrogen in the Sargasso Sea. Deep-Sea Research I 49, 1445–1461.

Sterner, W., Elser, J.J., 2002. In: Sterner, W., Elser, J.J. (Eds.), Ecological Stoichiometry: The Biology of Elements from Molecules to the Biosphere. Princeton University Press, Princeton, NJ.

Strom, S., Benner, R., Ziegler, S., Dagg, M., 1997. Planktonic grazers are a potentially important source of marine dissolved organic carbon. Limnology and Oceanography 42, 1364–1374.

Suess, E., 1980. Particulate organic carbon flux in the ocean-surface productivity and oxygen utilization. Nature 280, 260–263.

Sunda, W.G., Huntsman, S.A., 1995. Iron uptake and growth limitation in oceanic and coastal phytoplankton. Marine Chemistry 50, 189–206.

Sweeney, E., McGillicuddy, D.J., Buesseler, K.O., 2003. Biogeochemical impacts due to mesoscale eddy activity in the Sargasso Sea as measured at the Bermuda Atlantic Time Series (BATS) site. Deep-Sea Research II 50, 3017–3039.

Takeda, S., 1998. Influence of iron availability, on nutrient consumption ratio of diatoms in oceanic waters. Nature 393, 774–777.

Taylor, K.E., 2001. Summarizing multiple aspects of model performance in a single diagram. Journal of Geophysical Research 106, 7183–7192.

Timmermans, K.R., et al., 2005. Physiological responses of three species of marine pico-phytoplankton to ammonium, phosphate, iron and light limitation. Journal of Sea Research 53, 109–120.

Turley, C.M., Mackie, P.J., 1995. Bacterial and cyanobacterial flux to the deep ne Atlantic on sedimenting particles. Deep-Sea Research I 42, 1453–1474.

Tyrell, T., 1999. The relative influences of nitrogen and phosphorus on oceanic primary production. Nature 400, 525–531.

Urban, J.L., McKenzie, C.H., Deibel, D., 1993. Nanoplankton found in fecal pellets of macrozooplankton in coastal Newfoundland waters. Botanica Marina 36, 267–281.

Vallino, J.J., 2000. Improving marine ecosystem models: use of data assimilation and mesocosm experiments. Journal of Marine Research 58, 117–164.

Verity, P.G., Stoecker, D.K., Sieracki, M.E., Nelson, J.R., 1996. Microzooplankton grazing of primary production at 140°W in the equatorial Pacific. Deep-Sea Research II 43 (4–6), 1227–1256.

Waite, A.M., Safi, K., Hall, J., Nodder, S.D., 2000. Mass sedimentation of picoplankton embedded in organic aggregates. Limnology and Oceanography 45, 87–97.

Walsh, J.J., 1975. A spatial simulation model of the Peru upwelling ecosystem. Deep-Sea Research 22, 201–236.

Wu, J., Sunda, W., Boyle, E.A., Karl, D.M., 2000. Phosphate depletion in the western North Atlantic Ocean. Science 289, 759–762.

Zehr, J., Waterbury, J., Turner, P., Montoya, J., Omoregie, E., Steward, G., Hansen, A., Karl, D., 2001. Unicellular cyanobacteria fix N_2 in the sub-tropical North Pacific Ocean. Nature 412, 635–638.

Zhang, C., Zou, J., 1997. Nutrient uptake kinetics and growth under nutrient limitation of *Pseudonitzschia*. Oceanologia et Limnologia Sinica 28, 599–603.

Zhang, X., Dam, H.G., White, J.R., Roman, M.R., 1995. Latitudinal variations in mesozooplankton grazing and metabolism in the central tropical Pacific during the U.S. JGOFS EqPac study. Deep-Sea Research II 42 (2–3), 695–714.